Available online at www.sciencedirect.com
ScienceDirect
Lithos 103 (2008) 257–287
LITHOS
www.elsevier.com/locate/lithos

# Styles of post-subduction collisional orogeny: Influence of convergence velocity, crustal rheology and radiogenic heat production

Manuele Faccenda [a,*], Taras V. Gerya [a], Sumit Chakraborty [b]

[a] Institute of Geophysics, Swiss Federal Institute of Technology (ETH Zurich), CH-8092 Zurich, Switzerland
[b] Institut für Geologie, Mineralogie und Geophysik, Ruhr-Universität Bochum, D-44780 Bochum, Germany

Received 22 September 2006; accepted 3 September 2007
Available online 3 October 2007

**Abstract**

A number of models of continental collision already exist, but the role of foregoing oceanic plate subduction or variable coupling between plates still remains to be explored. In addition, heat generation by radioactive decay may be quite variable. For example, our geochemical data from low-to-high grade metamorphic rocks of the Lesser and Higher Himalayan sequences reveal measured heat production values on the order 4–5 $\mu W/m^3$, which is considerably higher than normal inferred upper crustal values ($<1.5$ $\mu W/m^3$). Therefore, we performed 2D numerical experiments of oceanic-continental subduction followed by continental collision for varying continental lower crustal strength, convergence velocity and radiogenic heating rate.

Oceanic subduction produces thinning and upwarping of the overriding lithospheric wedge, such as is observed in Andean-type collisional settings (Cascadia and Central Andes). After collision two main orogenic styles develop depending on the values of key parameters: either (a) slow convergence rates (weak shear heating and consequently strong rheological coupling between plates) and/or a weak lower crust generate a *two-sided*, thick and narrow symmetrical collisional zone, or (b) high convergence rates (strong shear heating and therefore weak rheological coupling between plates) and a strong lower crust produce a *one-sided*, thin and broad asymmetrical collisional zone. In this case a vertical lithospheric body divides two upper crustal wedges that develop distinct deformation patterns. In both cases, enhanced radiogenic heating favors the formation of midcrustal partially melted channels that propagate toward the surface and the pro-foreland. Partial melting triggers lateral extrusion of metamorphic rocks from different depths (15–23 kbar, $>700$ °C) on top of coherent LP-LT units. The geometry of metamorphic isograds (inverted), shapes of P-T paths at different grades and exhumation rates are similar to those observed in parts of the Himalayan chain, indicating that the models capture the essence of real systems. The model results demonstrate that internal heat production rate is a crucial parameter in determining the timing of slab breakoff, polarity reversal and exhumation of the inverted metamorphic sequence with respect to the timing of partial melting. Late stages of some numerical experiments showed interesting geodynamical evolution of the collisional zone, with the appearance of polarity reversal, roll over of both plates and roll back of the subducting slab. Irrespective of these details, hundreds of km of continental lithosphere are recycled into the mantle in all models, supporting the idea that continental crustal consumption is, indeed, a common and considerable process during collision. This affects inferences about extents of convergence and/or shortening during orogenesis. Moreover, crustal recycling into the deep mantle during collisional orogeny needs to be considered in models of crustal growth and evolution.


*Keywords:* Continental collision; Rheological coupling; Radiogenic heat; Crustal recycling; Numerical modeling; Partial melting

* Corresponding author. Tel.: +41 44 6337653; fax: +41 44 6331065.
*E-mail address:* manuele.faccenda@erdw.ethz.ch (M. Faccenda).

0024-4937/$ - see front matter © 2007 Elsevier B.V. All rights reserved.
doi:10.1016/j.lithos.2007.09.009

## 1. Introduction

The structure and geometry of collisional orogens on a lithospheric scale remains a complicated and poorly resolved aspect of plate tectonics. In the past years, field geologists and geophysicists have made important contributions to the understanding of collisional chain dynamics. Nevertheless, surface geological complexities and the lack of high resolution geophysical methods in most of the orogens leave ambiguities in the interpretation of the continental plates interplay. Andean-type collision is a well known geodynamical process, where a lower and denser plate underthrusts a gravitationally stable continent; on the other hand, Alpine-type collision is characterized by convergence of two buoyantly similar plates whose dynamical evolution is a nontrivial problem.

In recent years numerical modeling has been used widely to investigate convergence between continental plates (e.g. Beaumont et al., 2001; Pysklywek, 2001; Pfiffner et al., 2000; Burov et al., 2001; Burg and Gerya, 2005) and significant progress has been achieved in our understanding of orogenic processes. However, a majority of the numerical studies of collision are based on simplified models which do not address tectonic implications arising from a foregoing oceanic subduction (such as slab delamination and slab breakoff) and further efforts are still needed for understanding geodynamic controls and styles of post-subduction collisional orogenic processes (e.g. Gerya et al., 2008-this volume).

Modeling of collisional orogens also includes constraints from the thermal structure observed in mountain chains. Thermal models of collisional settings generally predict temperature structures that are much cooler than those recovered by thermobarometric studies (Huerta et al., 1998; Jamieson et al., 1998). Recently, Burg and Gerya, 2005, have contributed to the solution of the problem by pointing out the role of dissipative shear heating in convergent plate margin contexts; at the same time, their quantification of the magnitude of this effect clarifies that the heat budget problem is not solved. As shown in previous works (Chamberlain and Sonder, 1990; Huerta et al., 1998, 1999; Goffè et al., 2003; Jamieson et al., 1998), the accretion of material with a high concentration of radiogenic elements at the active margin is an additional heat source that can provide the amount of heat needed to obtain the observed peak temperatures.

In the course of a study of the geochemistry and petrology of Barrovian and adjacent metamorphic rocks spanning the lesser and higher Himalayan sequences in Sikkim (Eastern India) and Himachal Pradesh (Northwestern India), we found unusual enrichment of the radiogenic heat producing elements U and Th relative to mean upper crustal (UC) abundances (e.g. Rudnick and Fountain, 1995; Taylor and McLennan, 1995). For example, mean U (4 ppm, UC ~2.5–3 ppm) and Th (32 ppm, UC ~10 ppm) concentrations from bulk chemical analyses of 150 rocks ranging from chlorite phyllites to high grade migmatites in metamorphic grade imply at least a factor of two increase in heat generation over mean upper crustal values, as shown in Fig. 1. That metamorphic and igneous rocks of the Himalayan range have high concentrations of radiogenic elements has already been recognized by other authors (Vidal et al., 1982; Scaillet et al., 1990; Macfarlane, 1992). Furthermore, data from the precambrian Kanskiy Complex of Eastern Siberia (Nozkhin and Turkina, 1993) and Mesoproterozoic gneisses and granites of the Mount Painter Province, South Australia, reveal similar excesses of radiogenic heat producing elements (Neumann et al., 2000), suggesting that the existence of rocks enriched in radiogenic elements is not unusual and restricted to only the Himalayan units.

As the metamorphic rocks at the highest grades still contain such high concentrations of U and Th, these measured values must represent minimum values for concentrations of these heat producing elements that were available before and during metamorphism — any melt loss from the migmatites would have preferentially sequestered these rather incompatible elements. Indeed, from entirely different geophysical considerations, Cattin

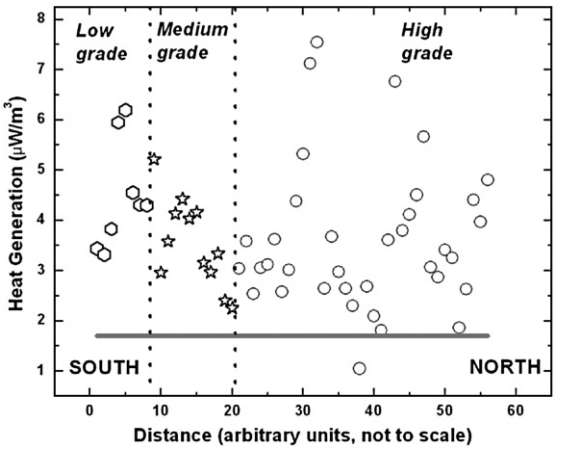


Fig. 1. Calculated heat generation (in $\mu W/m^3$) from 56 samples along a south to north traverse in the Sikkim Himalaya starting in the lesser Himalayan sequence from low grade chlorite — biotite grade metasediments (polygons) through medium grade (garnet — kyanite grade, stars) to higher Himalayan migmatitic, sillimanite grade and higher (circles) rocks. The gray line shows mean upper crustal heat generation of 1.7 $\mu m/m^3$ based on data from Rudnick and Fountain, 1995.

and Avouac (2000) concluded that high heat production in the upper crust is necessary to be consistent with seismic and geomorphological data of the Himalayan chain.

The observed heat generation from measured concentrations of U, Th and K in samples collected along the North–South transect in the Himalayas are on the order of 4–5 $\mu W/m^3$, which is considerably higher than the 2.5 $\mu W/m^3$ required by their models.

Lastly, and perhaps most importantly, there is a geological basis for considering high heat production in these settings. The fact that sediments in continental margins accumulate heavy minerals such as zircons and monazite that concentrate U and Th is a well known geological phenomenon. These would constitute some of the most likely material to be buried during subduction/collision processes so that the involvement of high heat generating materials in such settings should be expected. Once adequate heat sources have been identified, the role of localized density and viscosity reduction due to melting reactions (e.g. Pattino-Douce et al., 1990, and Pysklywek and Beaumont, 2004) needs to be considered in an integrated internally consistent thermo-mechanical model.

Bearing in mind these considerations and simplifications used in previous simulations, we have set up 75 2-D numerical experiments simulating subduction followed by continental collision. Our goal was twofold: (i) identifying and describing major styles of post-subduction collisional orogeny with this new type of numerical model and (ii) quantifying the possible influence of three major physical parameters (convergence rate, crustal rheology and radiogenic heat production) on orogenic styles.

We also compare our numerical predictions with natural observations in order to test the possibility of identification of these different orogenic styles in the nature. We note in this context that once key parameters guide the evolution of a system along certain paths (e.g. development of symmetric/asymmetric collision zones, rapid/slow exhumation of metamorphic rocks) in the early stages of collision, the resulting characteristics may be retained in the integrated field record from relatively mature orogenic belts (e.g. Himalaya) as well. Therefore, comparison of aspects of our models of early stages of collision with appropriate field records from such mature natural systems could constitute valid tests of the models.

## 2. Numerical modeling

2D thermo-mechanical models were employed using a finite-difference numerical code (I2VIS) with non-diffusive-marker-in-cell technique (Gerya and Yuen, 2003a). Our large scale $4000 \times 670$ km model includes upper mantle and assumes a spontaneously bending oceanic slab subducting at a prescribed convergence rate for around 1000 km, after which it is allowed to move freely underneath a continental upper plate (Fig. 2). We assume that dehydratation processes of such a short slab will have negligible effects on the overall evolution of the system, although the absence of continuous hydration and the resultant rheological weakening of the overriding plate during subduction (Gerya and Stöckhert, 2002) could increase friction between the plates in this pre-collisional setting.

In all subsequent discussion, the plate with an initial oceanic component is considered to be the "left plate" and the imposed motion is to the right. To distinguish different parts of the crustal collisional zone we have used the terminology adopted in Jamieson et al., 1998, where the prowedge indicates the part above the subducting slab and the retrowedge is mainly on the overriding plate.

The subducting oceanic slab is attached to a continental passive margin where a 10 km thick pile of radiogenic sediments is supposed to have accumulated by cratonic erosion (Fig. 2c). The model accounts for shear heating that has been shown to be an important component of the overall heat budget (Molnar and England, 1990, England et al., 1992, Burg and Gerya, 2005). The degree of rheological coupling between the two plates defined by the effective strength of rocks composing the plate interface is inversely proportional to the amount of heat produced at this shearing interface that, in turn, depends on the convergence velocity. Here we demonstrate that such shear heating is a fundamental parameter in determining orogenic styles of deformation.

The models include the effects of buoyancy forces and consider increased mobility due to partial melting of crustal rocks as well. A detailed description of the model and numerical techniques employed in our study is given in Appendix A. Uncertainties in our knowledge of composition of the lower continental crust translate to poorly constrained rheological behavior of this region. We adopted three different flow laws for the lower continental crust in order to simulate extreme variations in the strength of the continental lithosphere; a complete description of the lithologies used is shown in Table 1.

## 3. Model results

Following the logic outlined in the Introduction we conducted systematic numerical experiments covering broad ranges of variation for each of the three chosen physical parameters. Seventy-five ($5 \times 5 \times 3$) simulations

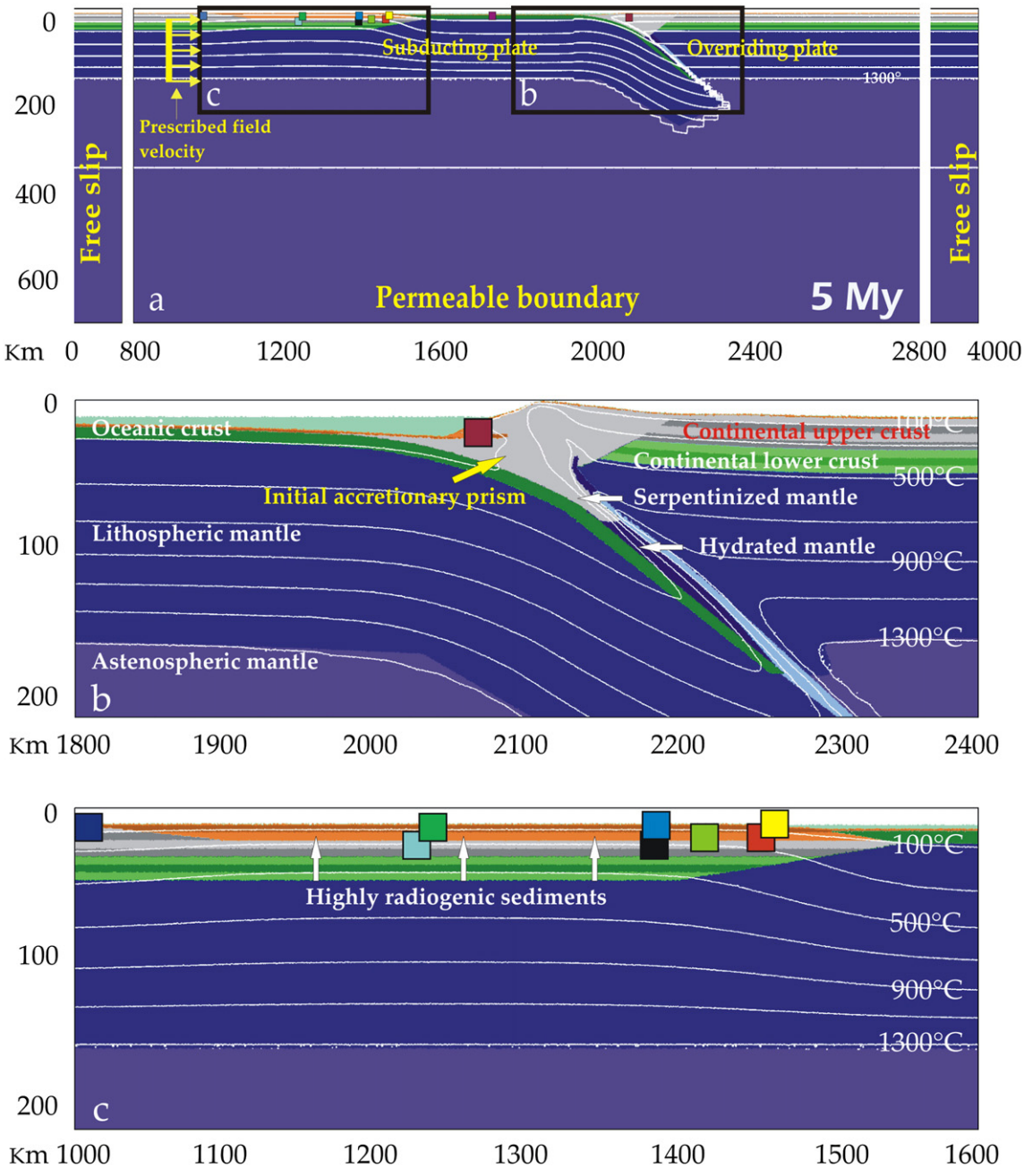


Fig. 2. Initial set up of the models: a) Enlargement (2000 × 700 km) of the numerical box (4000 × 700 km). Boundary conditions are indicated in red; the starting geodynamical setting is that of a young (5 Ma) oceanic subduction, with the left plate subducting under the right one. The prescribed field velocity is imposed at 900 km. b) and c) are zoomed areas of a showing the lithologies used. Coloured squares indicate the initial position of selected markers for P-T-t paths reconstruction of the reference model plagioclase, Vs = 7, Hr = 5. Color scale for the different lithologies is described in Fig. 3. c) denotes the occurrence of a 10 × 400 km layer of highly radiogenic sediments settled on the continental passive margin. White lines are isotherms measured in °C.

were carried out in order to investigate the effects of convergence rate (Vs = 2, 3, 5, 7, 10 cm/yr), radiogenic heat production of the passive margin sediments (Hr = 1, 2, 3, 4, 5 $\mu W/m^3$) and viscous rheology (= strength) of the lower crust (mafic granulite flow law = strong; plagioclase An75 flow law = medium; Wet Quartzite flow law = weak, Ranalli, 1995, and references therein, see Table 1).

Results are depicted in Figs. 3–15, where a model with lower crustal rheology corresponding to the plagioclase ($An_{75}$) flow law, imposed convergence velocity of 7 cm/yr and radiogenic heat production in

Table 1
Material properties used in 2D numerical experiments

| Material | $\rho_0$, kg/m$^3$ | k, W/(m K) | $T_{solidus}$, K | $T_{liquidus}$, K | $Q_L$, kJ/kg | $H_r$, μWm$^3$ | Flow law | $E$, kJ/mol | $n$ | $A_D$, MPa$^{-n}$·s$^{-1}$ | $V$, J/(MPa·mol) | $\mu$, GPa |
|---|---|---|---|---|---|---|---|---|---|---|---|---|
| Continental upper crust, sediments | 2800 (solid) 2500 (molten) | $[0.64+807/(T+77)]\times\exp(0.00004\ P_{MPa})$ | $889+17900/(P+54)+20200/(P+54)^2$ at $P<1200$ MPa, $831+0.06\ P$ at $P>1200$ MPa | $1262+0.09P$ | 300 | 1.0–5.0 | Wet quartzite | 154 | 2.3 | $10^{-3.5}$ | 0 | 10 |
| Continental lower crust | 3000 (solid) 2900 (molten) | $[1.18+474/(T_K+77]\times\exp(0.00004\ P_{MPa})$ | $973-70{,}400/(P+354)+77{,}800{,}000/(P+354)^2$ at $P>1600$ MPa, $935+0.0035\ P+0.0000062\ P^2$ at $P<1600$ MPa | $1423+0.105P$ | 380 | 0.25 | Wet quartzite | 154 | 2.3 | $10^{-3.5}$ | 0 | 10 |
| | | | | | | | Plagioclase An75 | 238 | 3.2 | $10^{-3.5}$ | | 25 |
| | | | | | | | Mafic Granulite | 445 | 4.2 | $10^{4.1}$ | | – |
| Oceanic crust | 3000–3100 (solid) 2900 (molten) | $[1.18+474/(T_K+77]\times\exp(0.00004\ P_{MPa})$ | $973-70{,}400/(P+354)+77{,}800{,}000/(P+354)^2$ at $P<1600$ MPa, $935+0.0035\ P+0.0000062\ P^2$ at $P>1600$ MPa | $1423+0.105P$ | 380 | 0.25 | Plagioclase An75 | 238 | 3.2 | $10^{-3.5}$ | 0 | 25 |
| Lithosphere–asthenosphere dry mantle | 3300 | $[0.73+1293/(T_K+77]\times\exp(0.00004\ P_{MPa})$ | – | – | – | 0.022 | Dry olivine | 532 | 3.5 | $10^{4.4}$ | 8 | 67 |
| Hydrated mantle in subduction shear zone | 3000–3300 | $[0.73+1293/(T_K+77]\times\exp(0.00004\ P_{MPa})$ | – | – | – | 0.022 | Wet olivine | 470 | 4 | $10^{3.3}$ | 8 | 67 |
| References [b] | 1, 2 | 3 | 4 | 4 | 1, 2 | 1 | 5 | 5 | 5 | 5 | 1, 5 | 1 |

Cp=1000 J kg$^{-1}$ K$^{-1}$, $\alpha=3\times10^{-5}$ K$^{-1}$, $\beta=1\times10^{-5}$ MPa$^{-1}$ for all rock types.
1 = (Turcotte and Schubert, 1982); 2 = (Bittner and Schmeling, 1995); 3 = (Clauser and Huenges, 1995); 4 = (Schmidt and Poli, 1998); 5 = (Ranalli, 1995 and references therein).

passive margin sediments of 5 μW/m$^3$ is taken as the reference model (Fig. 3). A shorthand convention used to refer to this model is: plagioclase, Vs=7, Hr=5; other models are referred by analogous sets of key variable parameters. After detailed description of the reference model we discuss results of several other numerical experiments in order to characterize major post-subduction collisional orogenic styles identified by our study. A second objective of this sequential description is to quantify the individual roles of the three variable physical parameters in controlling the development of different orogenic styles.

### 3.1. Models description

#### 3.1.1. Reference model — plagioclase, Vs=7, Hr=5 (Figs. 3–6)

As a reference model, we chose an intermediate strength for the lower crust (plagioclase An75 flow law), a moderate to high convergence velocity typical of an Andean type convergent margin, and, in the light of our laboratory analysis, a high radiogenic heat production rate.

In the early stages of oceanic subduction (10 Ma), the upper plate is slightly upwarped by accretion of sediments and is poorly delaminated at the base due to mechanical shearing. Upwarping produces a lithospheric backstop for the accretionary complex where continental upper crustal rocks are mixed together with upper mantle and oceanic crust slices in a corner flow-like mass circulation.

At the onset of continental collision (15 Ma), the thick sedimentary layer of the downgoing plate is accreted at the active margin and the upper plate lithospheric wedge is pushed further backward and vertically tilted. The left plate, while it is still pushed horizontally by the imposed velocity field and vertically by slab pull, cannot sink much deeper due to the intrinsic buoyancy of continental crust; horizontal

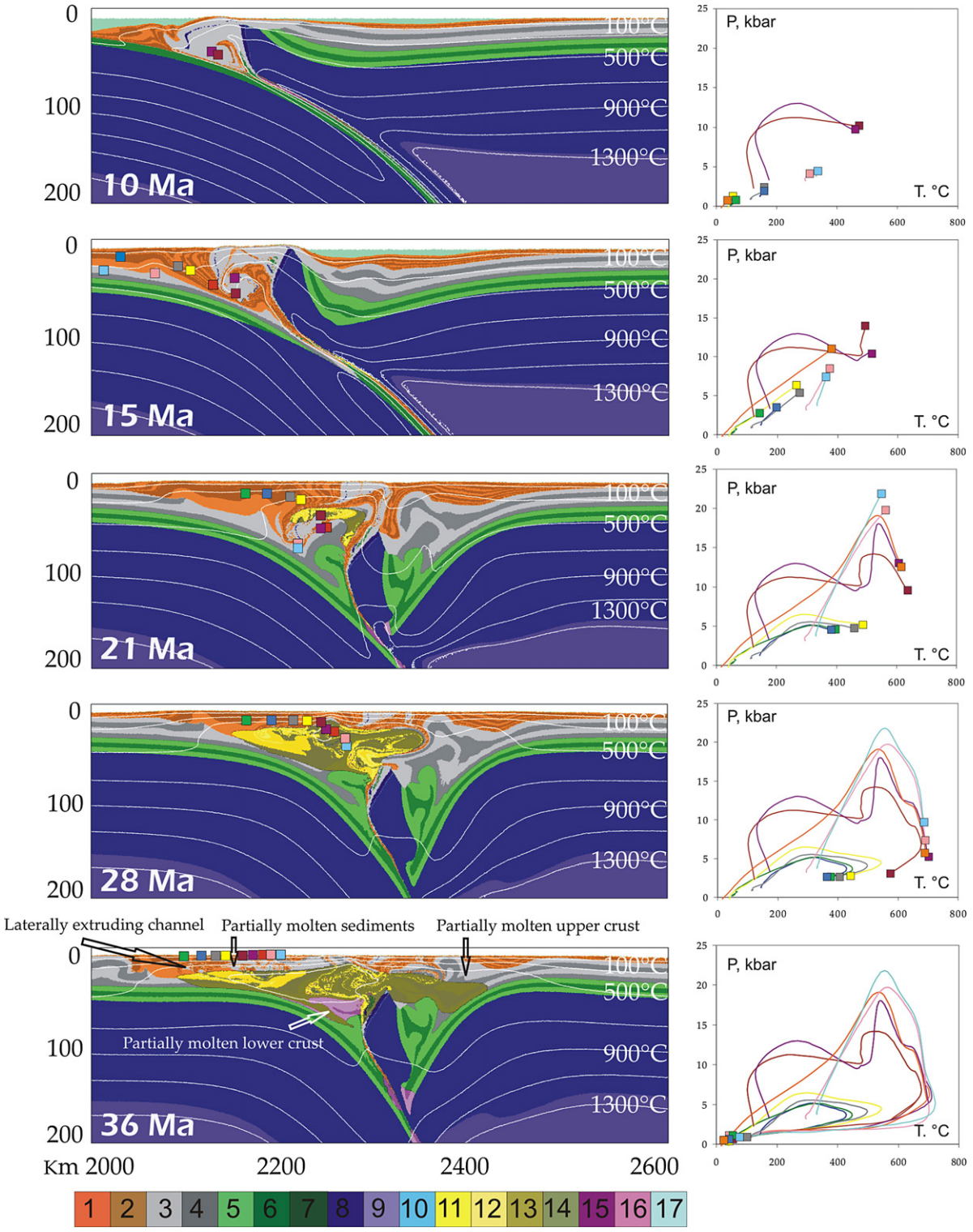


Fig. 3. Plagioclase Vs=7, Hr=5. (Left) Zoomed development of the reference model showing the yielding of the overriding slab at 21 Ma and the extrusion of a midcrustal partially melted channel that triggers exhumation of an inverted metamorphic sequence. (Right) P-T-t paths of markers selected at the surface at 36 Ma; the metamorphic grade increases toward the chain. The white lines are isotherms measured in °C. Color scale: 1,2: stratified sediments; 3,4: stratified upper crust; 5,6: stratified lower crust; 7: oceanic crust; 8: lithospheric mantle; 9: asthenospheric mantle, 10: serpentinized/hydrated mantle; 11,12: partially molten sediments; 13, 14: partially molten upper crust; 15,16: partially molten lower crust; 17: sea water.

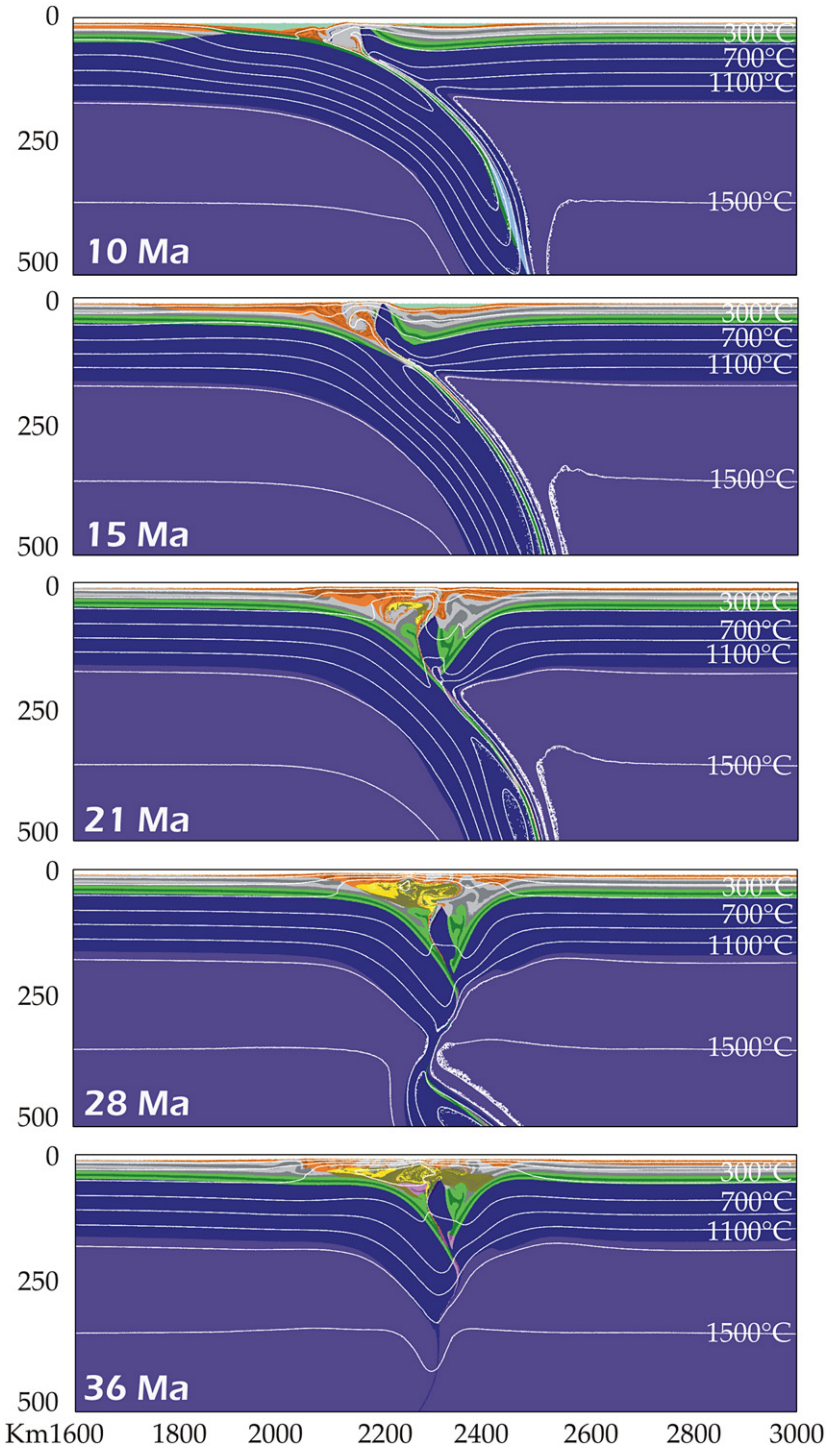


Fig. 4. Larger scale view of the same, reference simulation shown in Fig. 3 (plagioclase Vs=7, Hr=5). showing yielding of overriding slab and breakoff of underthrusting slab. Isotherms and color scale as in Fig. 3.

stresses, hence, are increased and the overriding slab buckles, giving rise to a *two-sided* collision overlain by a narrow and thick symmetric collision zone with a central and deeply buried lithospheric body (21 Ma).

The thick layer of highly radiogenic sediments piled at the active margin favors rising of isotherms and the midcrustal partial melting of sediments — crustal rocks that were formerly scraped off from the

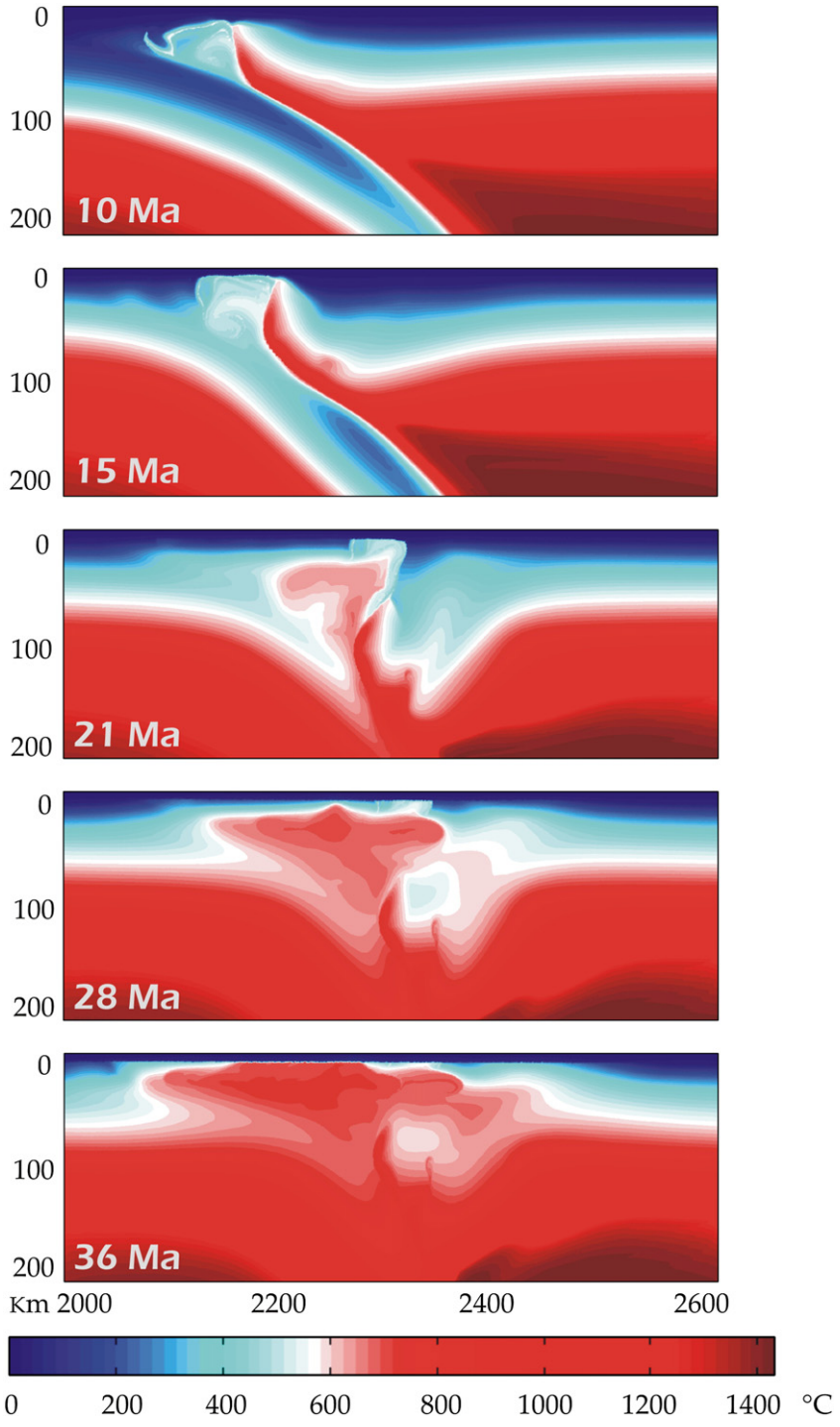


Fig. 5. Plagioclase Vs=7, Hr=5 reference model, same area and simulation as shown in Fig. 3. Zoomed distribution of peak temperature isograds. Peak temperature isograds clearly indicate lateral extrusion of a coherent metamorphic body.

subducting plate. The system is now almost mechanically stable, i.e. collision is nearly halted while the negatively buoyant subducted oceanic plate is still pulling downward. As a result, significant stretching forces are imposed onto the slab. This causes slab necking enhanced by the lowering of stress- and temperature-dependent mantle viscosity in the necking zone that subsequently leads to slab detachment (e.g.,

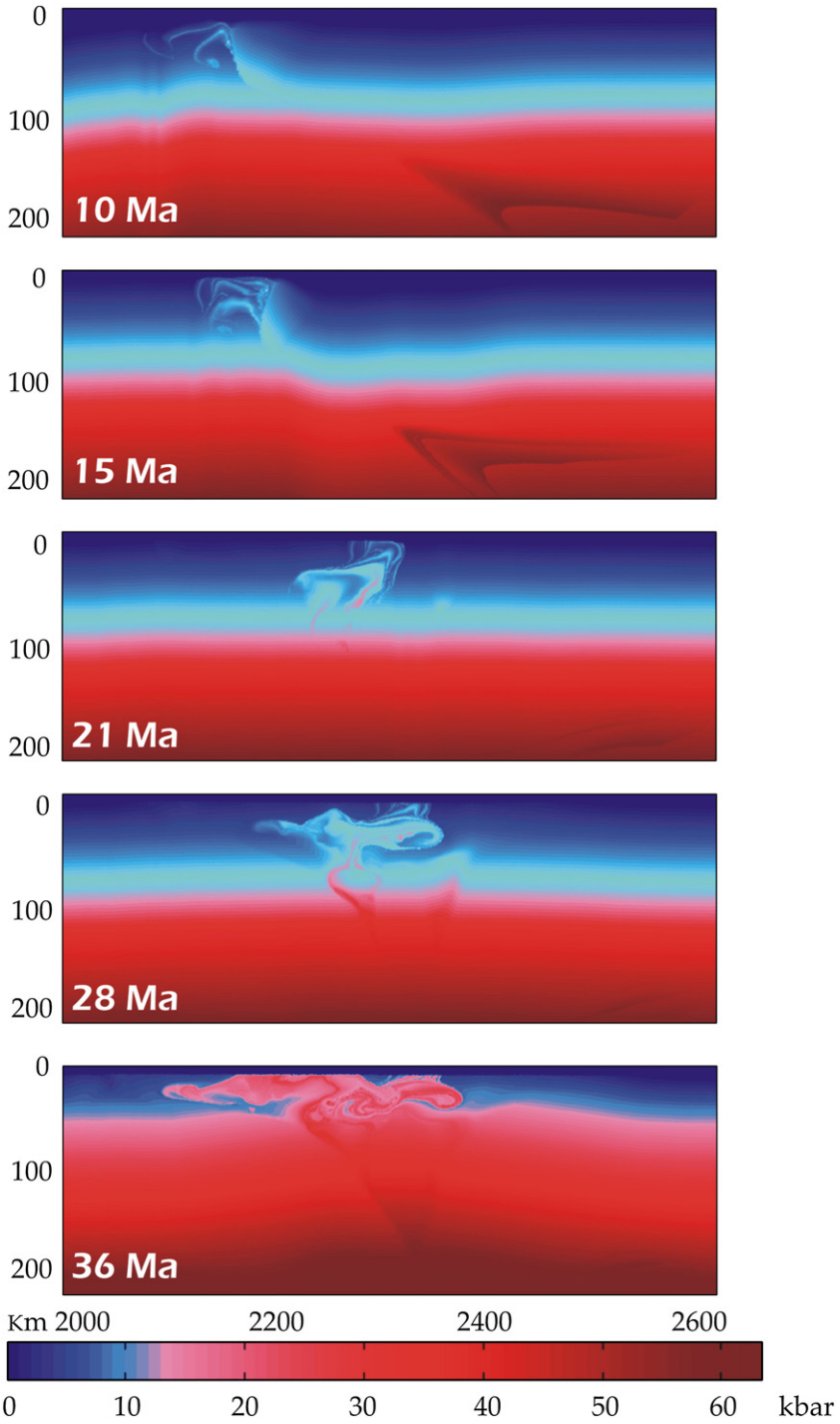


Fig. 6. Plagioclase Vs=7, Hr=5, reference model, same area as in Figs. 3 and 5. Zoomed distribution of the peak pressure isograds. Peak pressure isograds indicate lateral extrusion of a medium-to-high grade metamorphic body composed of rock units derived from different depths.

Gerya et al., 2004a) followed by isostatic rebound (28 Ma) (Fig. 4).

At shallow depths, the partially melted zone diffuses in the collisional wedge assuming a mush-room shape (28 Ma); diffusion is directed principally toward the surface (with emplacement of dome structures) and horizontally along the pro- and retro-forelands. Figs. 5 and 6 show the distribution of peak

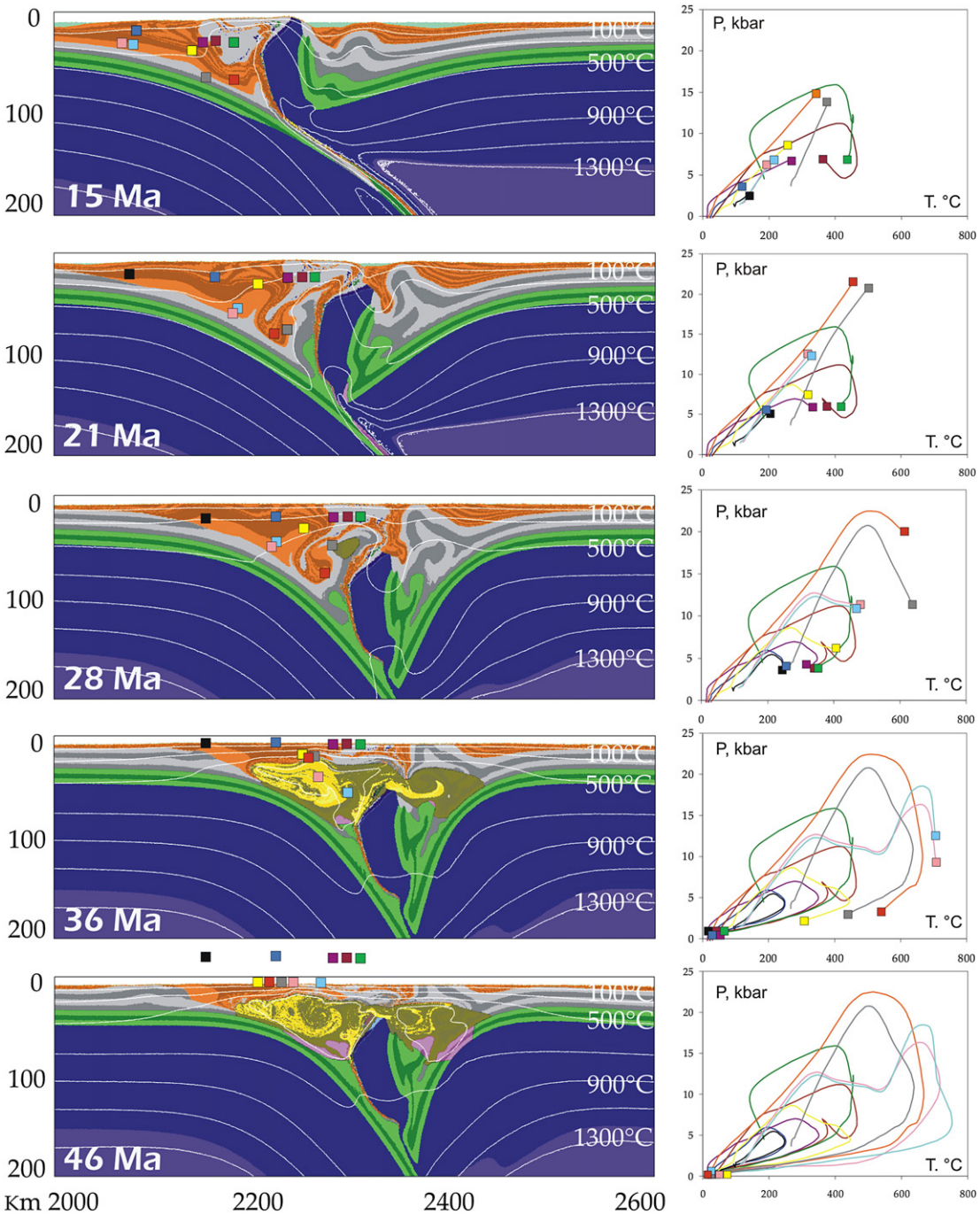


Fig. 7. Plagioclase Vs=7, Hr=2. (Left) Zoomed development of a model with a lower radiogenic content of the sediments compared to the reference model. The images show the overriding slab yielding at 21 Ma and the delayed (about 10 Ma) extrusion of a midcrustal partial melted channel that triggers exhumation of an inverted metamorphic sequence. (Right) P-T-t paths of markers selected at the surface at 36 Ma (heavy colours) and 46 Ma (light colours); at 36 Ma, markers selected at the surface retain a low metamorphic overprint; after 10 Ma, these markers are eroded (placed out of the last image, 46 Ma) and replaced by high grade metamorphic rocks. Isotherms and color scale as in Fig. 3.

T and P isograds, respectively, (that is, maximum temperature and pressure reached by a rock during its evolution). Peak temperature records suggest the lateral extrusion of a coherent elongated body; on the other hand, peak pressure signatures indicate notable mixing of rocks derived from different

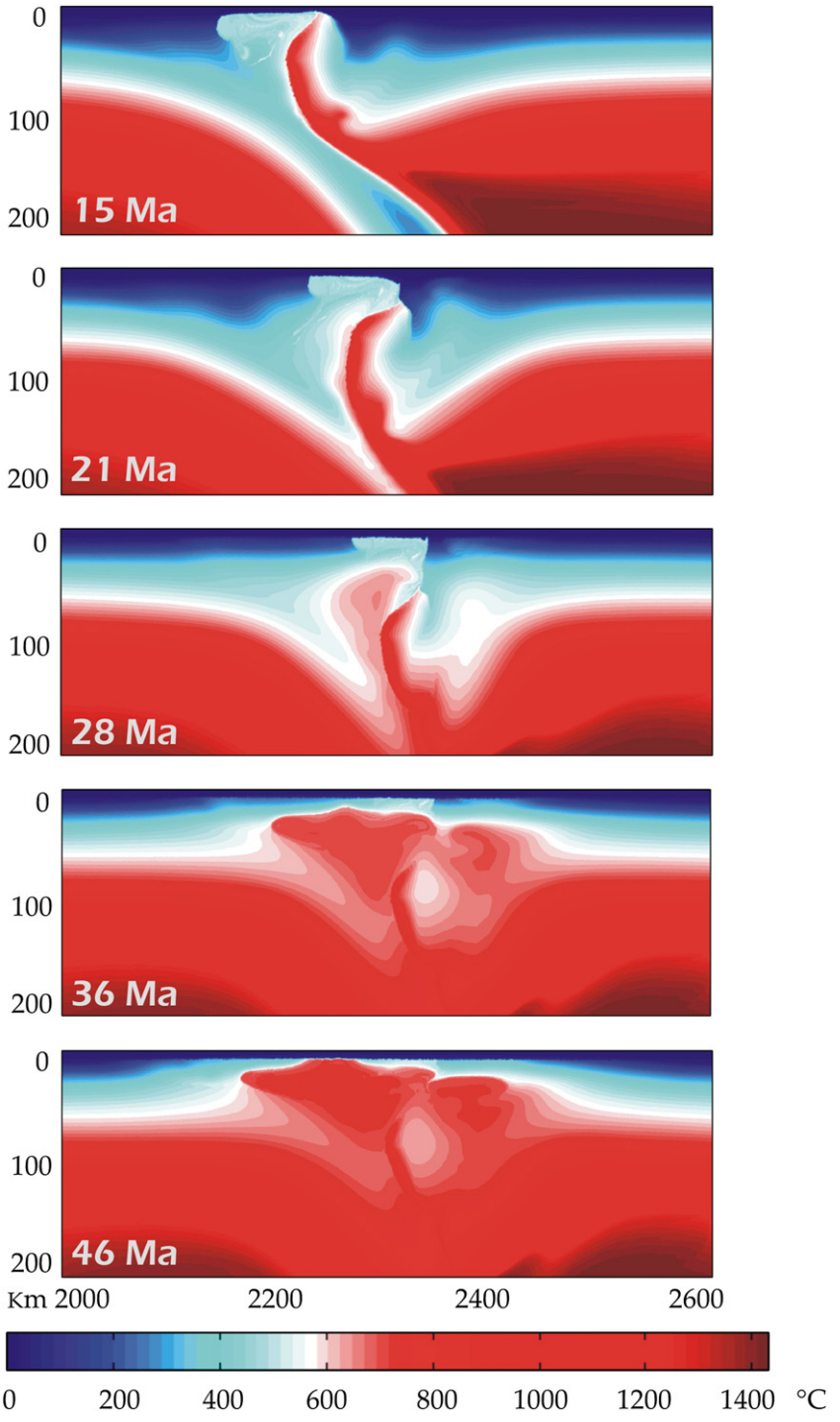


Fig. 8. Plagioclase Vs=7, Hr=2. Zoomed distribution of the peak temperature isograds of the model shown in Fig. 7. Peak temperature isograds indicate the delayed (10 Ma with respect to the reference model, Fig. 5) lateral extrusion of a coherent metamorphic body, though of smaller dimensions.

maximal depth levels. Partial melting decreases the density of crustal rocks triggering gravitational instabilities (Gerya et al., 2004b) that lead to the exhumation of high-grade metamorphic complexes from various depths (15–23 kbar, >700 °C) on top of a coherent block of low-grade units (36 Ma).

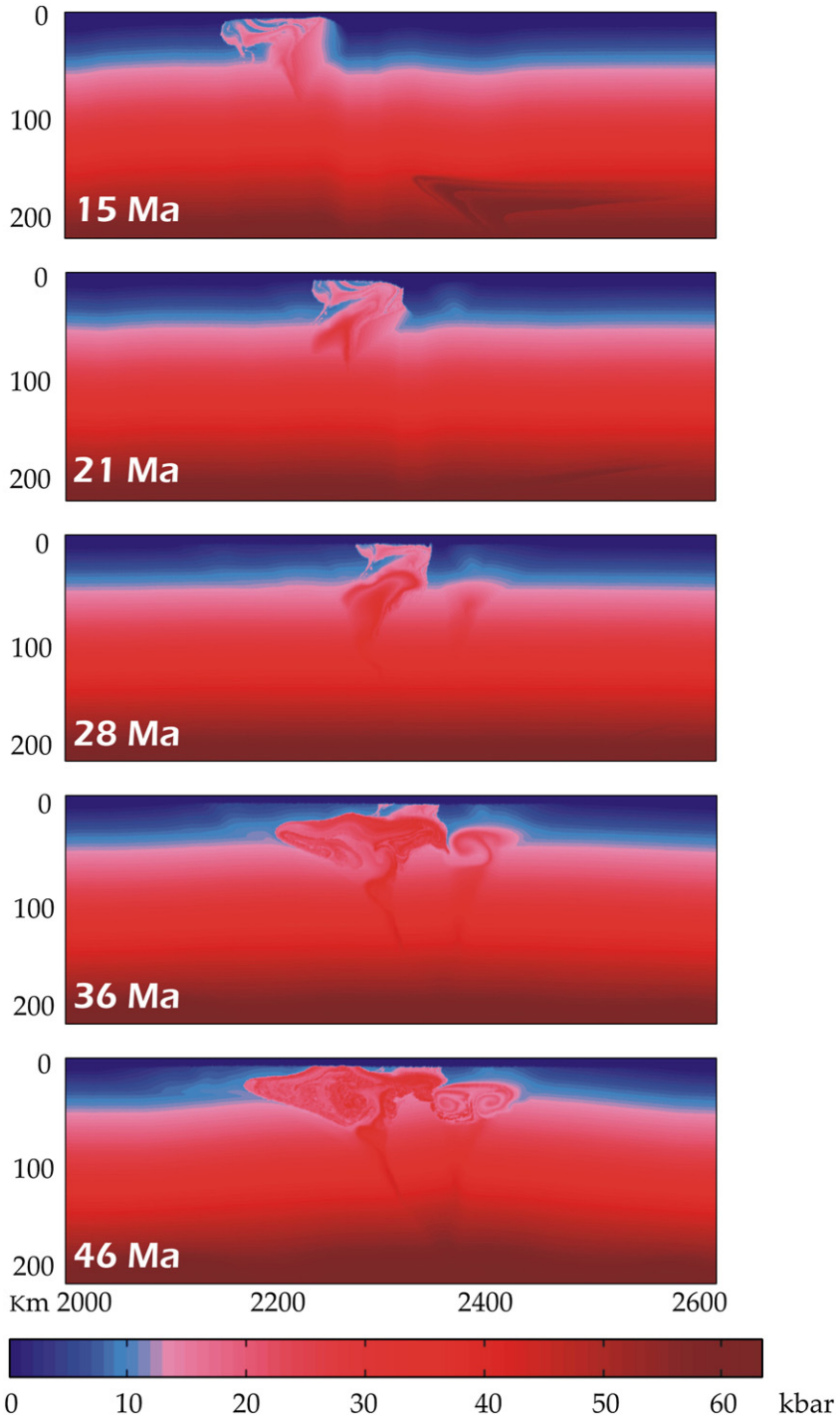


Fig. 9. Plagioclase Vs=7, Hr=2. Zoomed distribution of the peak pressure isograds of the same model as in Fig. 7. Peak pressure isograds indicate the delayed (10 Ma with respect to the reference model, Fig. 6) lateral extrusion of a medium-to-high grade metamorphic body with rocks from different depths, though of smaller dimensions.

*3.1.2. Lower radiogenic heat production — plagioclase, Vs=7, Hr=2 (Figs. 7–9)*

The second model differs from the reference model in that the passive margin sedimentary layer has 2.5 times lower concentration of radiogenic elements.

As shown in Fig. 7, tectonics at lithospheric scale is practically identical to that observed for the reference

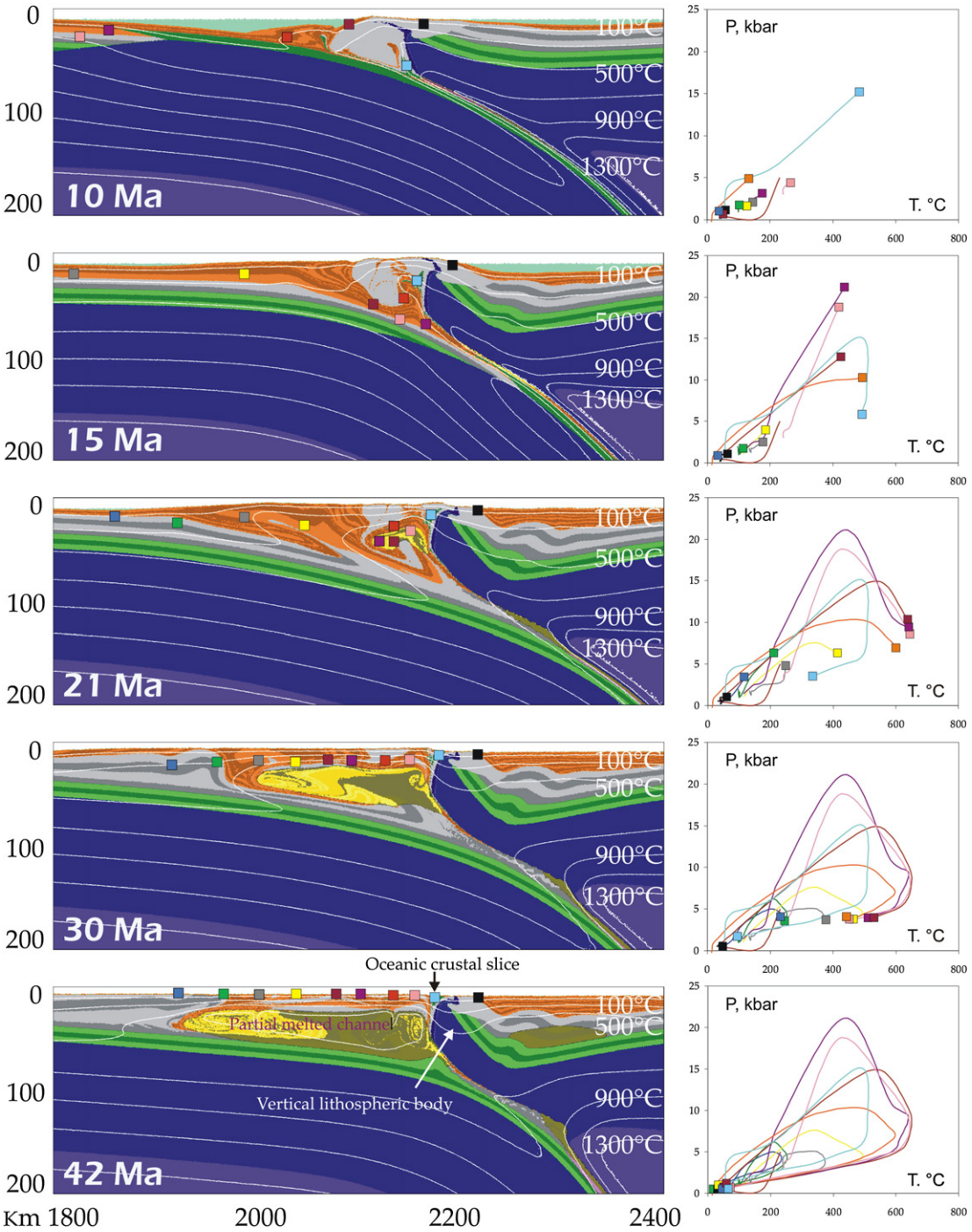


Fig. 10. Mafic granulite Vs=7, Hr=4. (Left) Zoomed development of a model with larger strength of the lower crust compared to the reference model. The upper plate does not yield, forming a wide and thin asymmetrical one-sided collisional zone where a sub-vertical lithospheric body separates two upper crustal wedges that develop different deformation styles (see text). An extruding midcrustal partially melted channel triggers exhumation of an inverted metamorphic sequence. (Right) P-T-t paths of markers selected at the surface at 42 Ma; the metamorphic grade is increasing toward the chain. Isotherms and color scale as in Fig. 3.

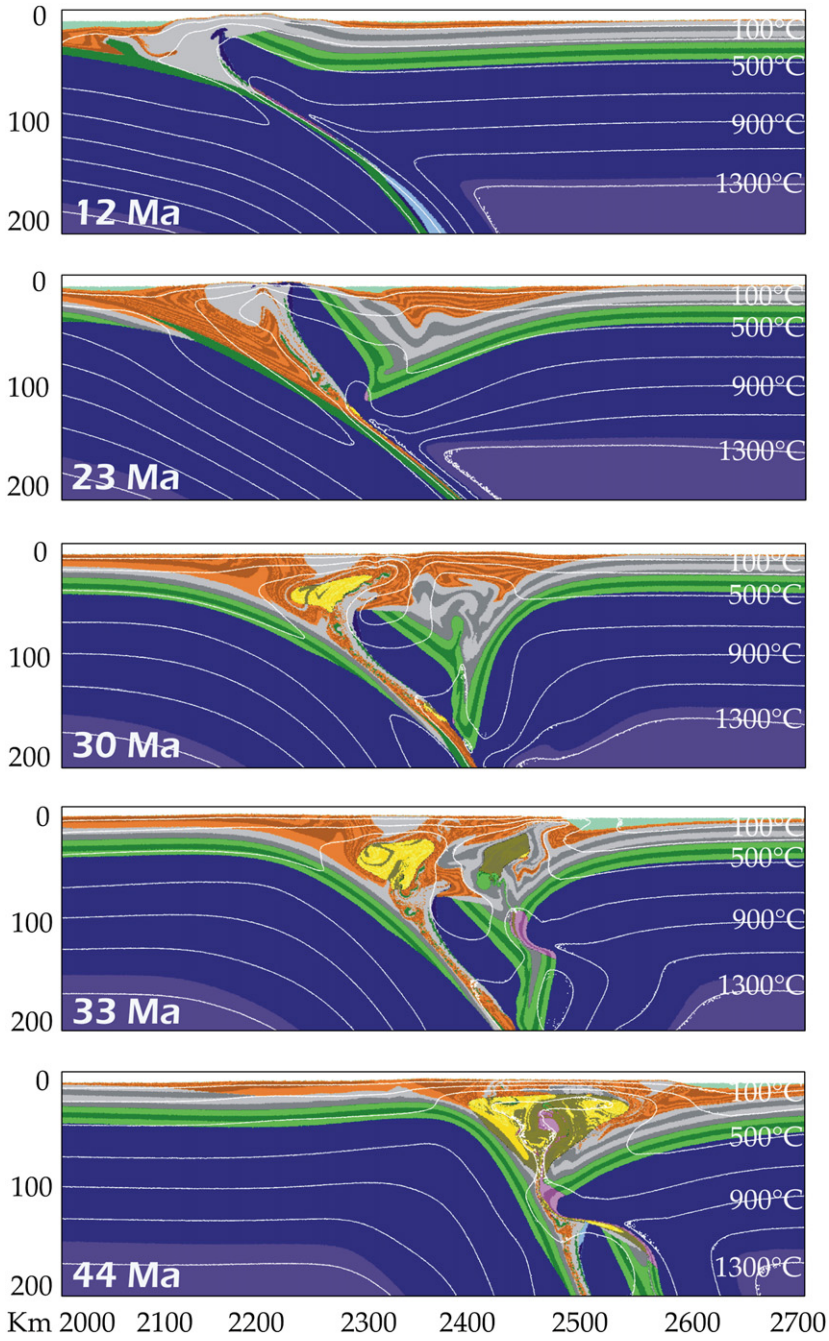


Fig. 11. Mafic granulite Vs=3, Hr=4. (Left) Zoomed development of a model with slower convergence rate and stronger lower crust with respect to the reference model. Shear heating produced at the shearing interface is too low and therefore the plates are strongly rheologically coupled. The stiff upper plate yields giving rise to a two-sided collision. Isotherms and color scale as in Fig. 3.

model at the same time steps (though slab detachment occurs 11–12 Ma later). However, a substantial difference is found in the thermal structure of the collisional zone that appears to be much colder; evidence is seen in the late occurrence of partial melting (28 Ma, Fig. 7, instead of 21 Ma of the reference model, Fig. 3) and the lower metamorphic grade of exhumed rocks. At 36 Ma, in fact, markers (rock units) selected at the surface have experienced only LP-LT conditions, whilst those exhumed at 46 Ma exhibit medium to high

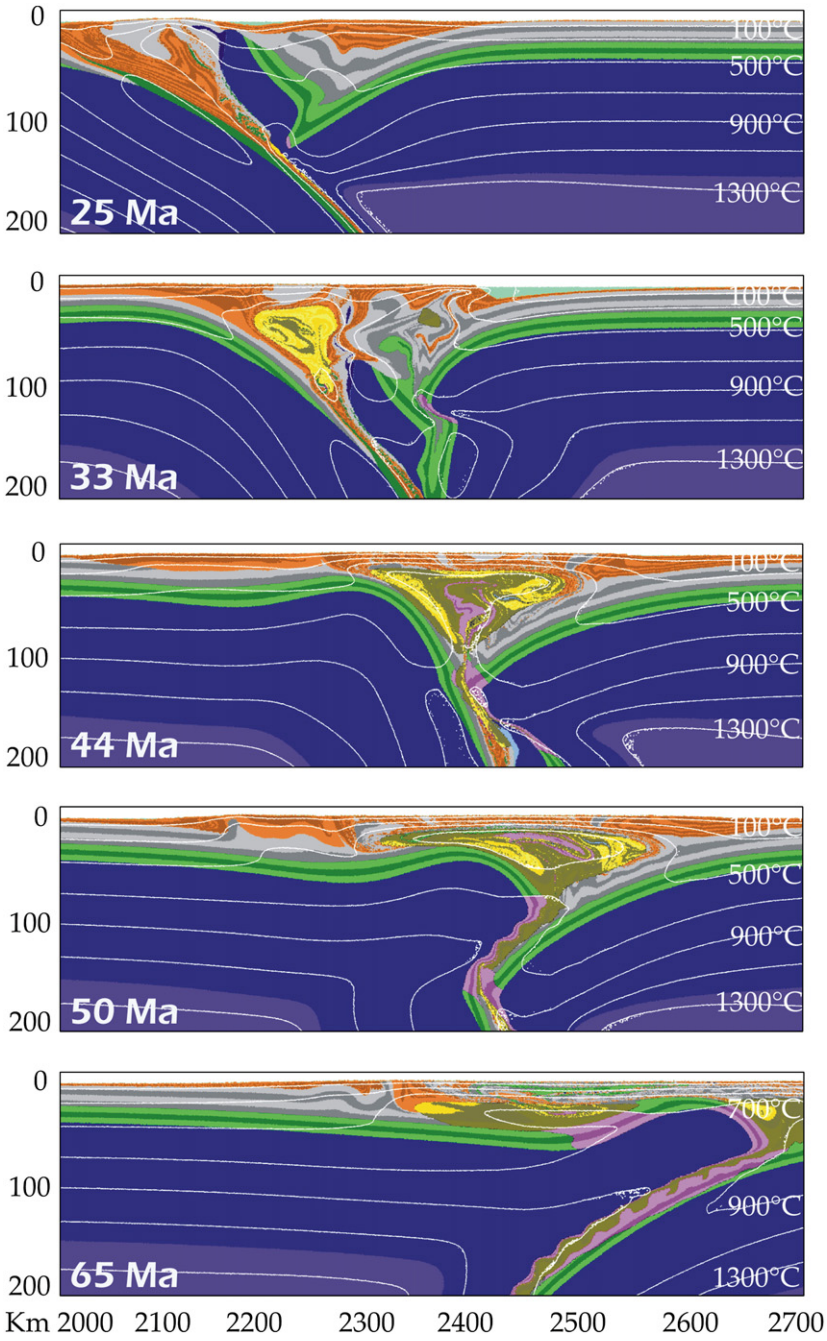


Fig. 12. Plagioclase Vs=3, Hr=5. Zoomed development of a model with a slower convergence rate with respect to the reference model. After the stabilization of a two-sided subduction zone, the lower slab suffers thermal weakening at the indentation zone (44 Ma). Being pushed by the imposed velocity field, the left plate starts to override the upper slab with the appearance of subduction reversal polarity (50–65 Ma). Isotherms and color scale as in Fig. 3.

metamorphic grade, indicating a time delay of about 10 Ma to obtain the same metamorphic isograd geometry as in the reference model (Figs. 8 and 9). This can be explained considering the delayed appearance of partial melting that, as shown before, triggers the final exhumation of medium-to-high grade metamorphic rocks. Lowered crustal temperature also causes the observed delay in the slab detachment since the timing of this process always increases with decreasing temperature at the top of the slab (Gerya et al., 2004a).

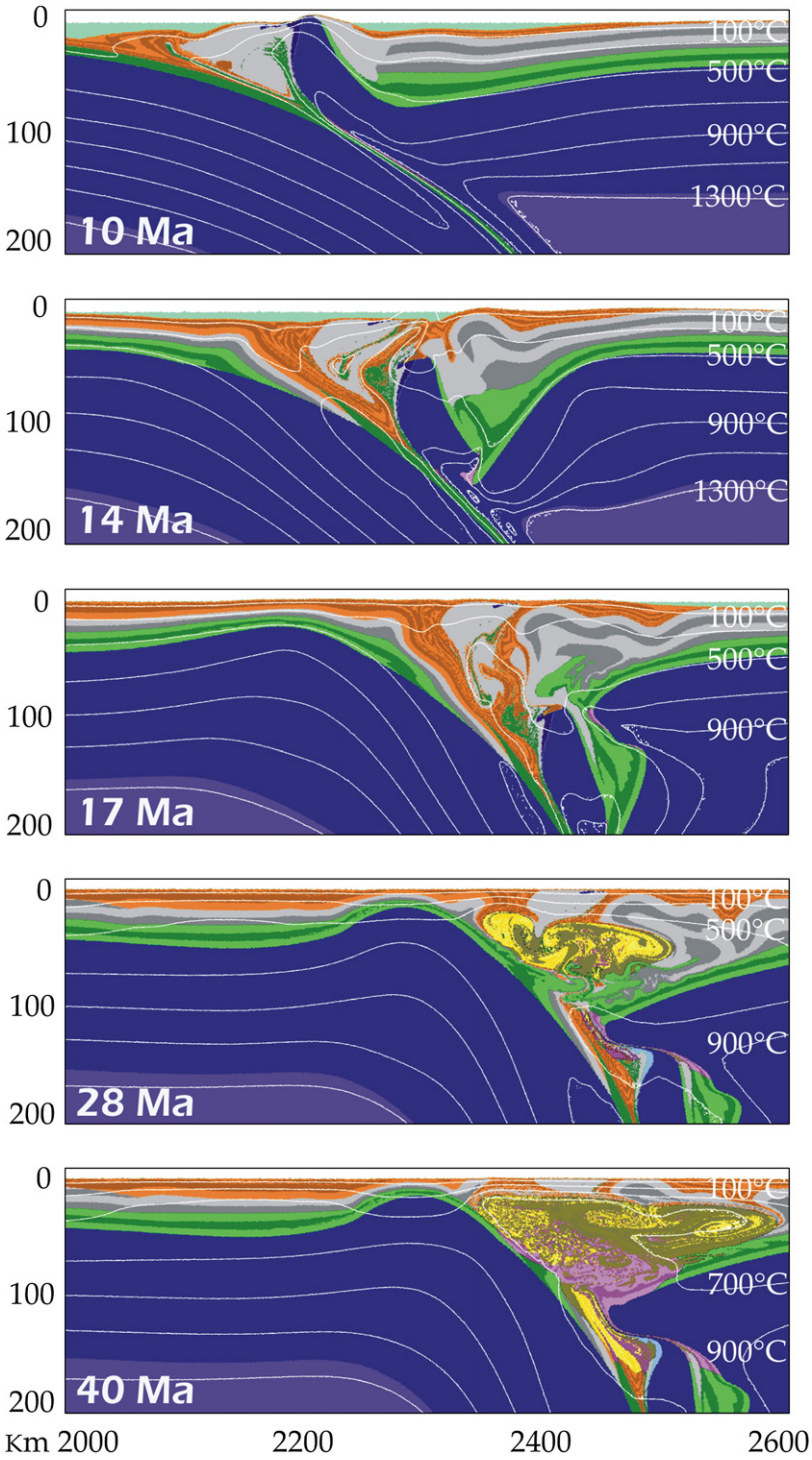


Fig. 13. Wet quartzite Vs=7, Hr=5. Zoomed development of a model with a weaker continental lower crust compared to the reference model. Upper slab yields before the collision (14 Ma). At 28 Ma, the lower plate is indented on the upper slab achieving mechanical stability. Isotherms and color scale as in Fig. 3.

*3.1.3. Stronger lower crust — mafic granulite, Vs = 7, Hr = 5 (Fig. 10)*

This experiment differs from the reference model in the choice of a stronger ductile flow law for the lower crust corresponding to that for a mafic granulite.

The initial development of the collisional zone is very similar to the previous models, with the upper plate

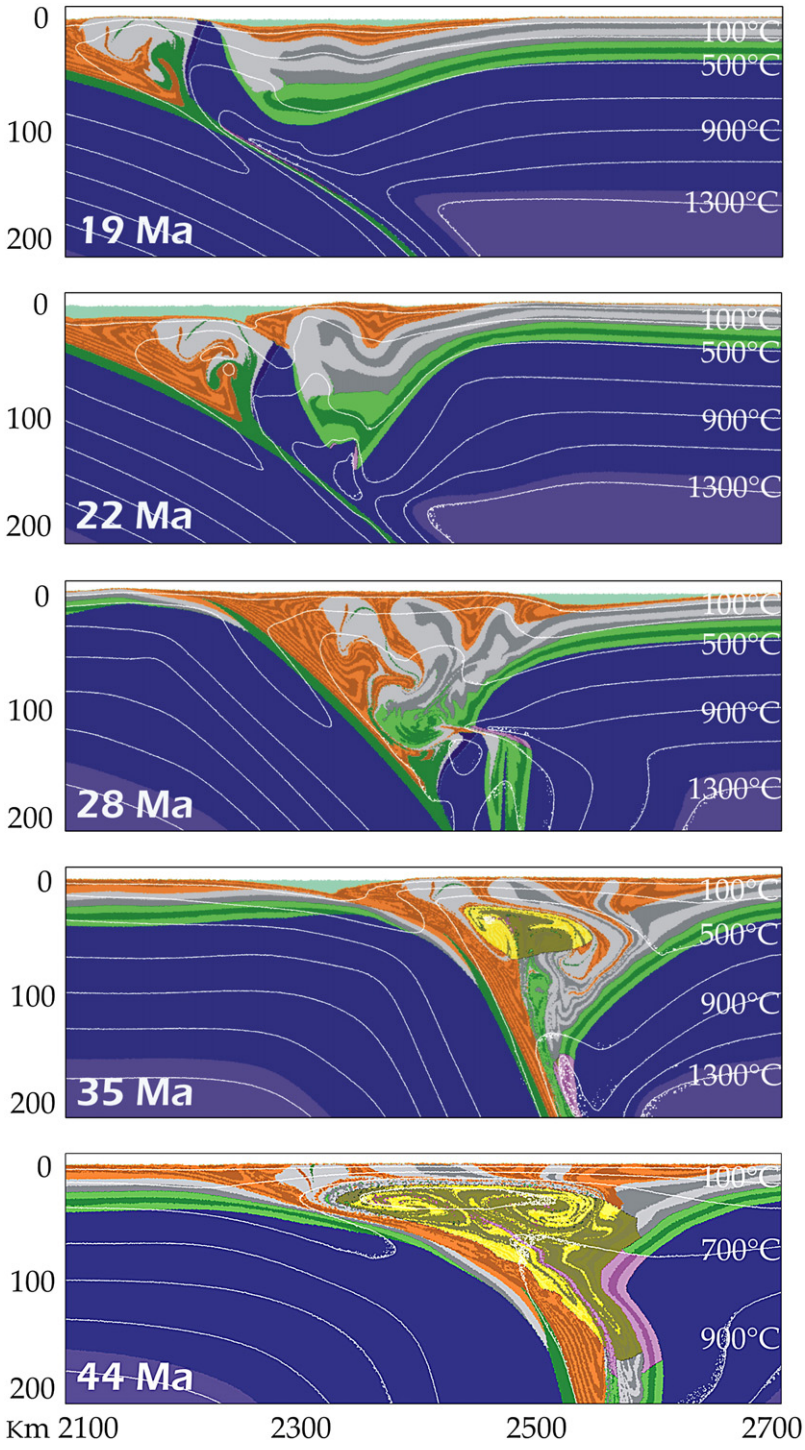


Fig. 14. Wet quartzite Vs=3, Hr=4. Zoomed development of a model with a weaker continental lower crust and slower convergence rate compared to the reference model. The lower plate is indented on the yielded slab and, because of the strong coupling, is able to overcome the resistance of the left plate and rolling over occurs (35 Ma, see text). Isotherms and color scale as in Fig. 3.

being only slightly ablated and thinned because of high shearing between the two plates that, therefore, are almost fully decoupled.

At the onset of continental collision (15 Ma) the left plate edge is warped upward due to the push from the material of the accretionary prism; however, in this

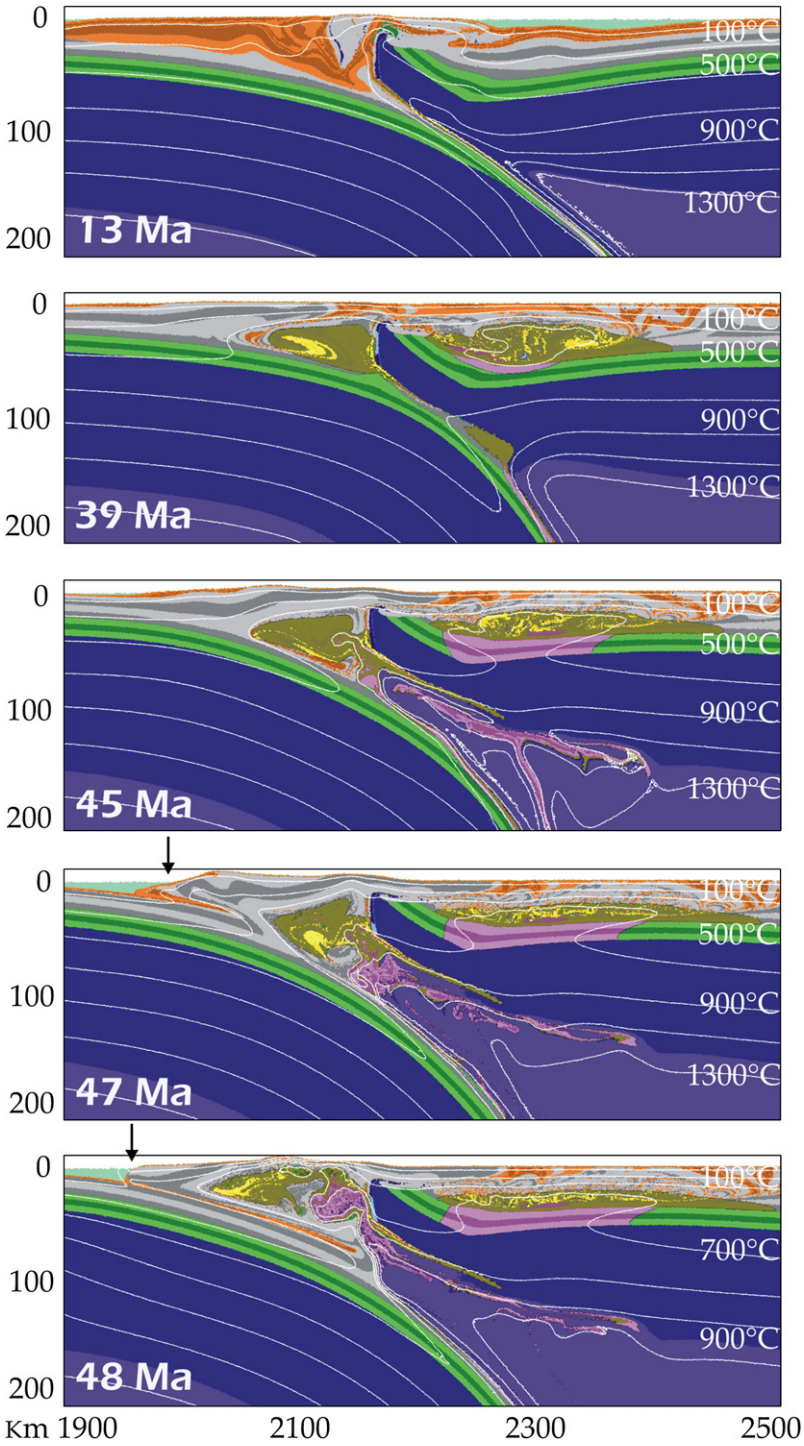


Fig. 15. Mafic granulite Vs=10, Hr=4. Zoomed development of a model with larger strength of the continental lower crust and higher convergence rate compared to the reference model. The general development resembles Mafic Granulite Vs=7, Hr=4 (Fig. 10), with convergence of two decoupled plates. At a later stage, slab pull causes roll back of the subducting plate with the formation of a post-collisional channel. Black arrows at 47 and 48 Ma indicate the edge of the thrusted upper crust: the mountain chain is propagating toward the pro-foreland. Isotherms and color scale as in Fig. 3.

case the overriding slab is strong enough to sustain stresses arising from collision and does not yield. Later on, the buoyancy of the continental crust slows down the convergence (21 Ma), though a nonnegligible part of continental lithosphere is still being subducted at the trench; the wide collisional zone achieves an asymmetric *one-sided* structure with the lithospheric edge acting as a buttress (due to the high rheological contrast between mantle and crustal rocks) and separating two wedges characterized by different deformation styles. The prowedge (on the left) is dominated by simple shear deformation, where the continental crustal material is wound up and stretched in a marble-cake fashion (Gerya and Stöckhert, 2006) together with oceanic crust (highlighted in Fig. 10 by a light blue square) and peridotitic slices; a partially melted zone appears at 21 Ma and propagates in the pro-foreland triggering final exhumation of an inverted metamorphic sequence with HP-MT rocks thrusted on LP-LT units (42 Ma). On the other hand, the retrowedge (on the right) is characterized by pure shear thickening of the crust, backthrusting and vertical exhumation/burial of material, no metamorphic overprint and the late formation of small volumes of partially molten crust due to the lack of a thick pile of radiogenic sediments.

The difference in the thermal evolution of the pro- and retrowedge in this case nicely underscores the significance of radiogenic material in controlling the peak metamorphic conditions that are attained by any given block of the crust. Also notable is the constitution of the suture zone, which is composed of HP-MT oceanic and continental crust as well as of peridotitic mantle that outcrops at the surface forming a complex structural pattern.

### *3.1.4. Stronger lower crust and slower convergence rate — mafic granulite, Vs = 3, Hr = 4 (Fig. 11)*

To demonstrate *counteracting effects* of simultaneous changes in two physical parameters we describe now results derived from a model including both a stronger rheology of the lower crust and a slower convergence rate compared to the reference model. Compared to the previous case, this simulation allows the isolation of the effect of slower convergence rate in a model with high strength of the lower crust.

In contrast to the previous experiment, in the early stages of subduction, the lithospheric mantle rocks from the bottom of the overriding plate are intensively dragged down together with the subducting plate (cf. displacement of dark blue material in Fig. 11, 12 Ma), indicating, thus, that the two plates are strongly rheologically coupled. At 30 Ma, the continental lower plate collides and drags downward part of the buckled overriding plate so that several hundreds of km of continental crust are consumed and placed in the lithospheric root (44 Ma).

The collisional zone is finally characterized by a symmetric *two-sided* structure (i.e. rather similar to the reference model) with a pro- and a back-side deformation pattern, a diffuse and inverted triangle shaped partially melted zone, and two downdipping slabs with the lower one indented onto the other.

The present model shows, hence, that even a strong lithosphere yields when plates converge at slow velocities; strong *rheological coupling* between the plates (defined by the effective strength of rocks composing the plate interface) is, then, a direct consequence of the small amount of viscous heating produced at the slowly shearing interface (Burg and Gerya, 2005).

### *3.1.5. Slower Convergence rate — plagioclase, Vs = 3, Hr = 5 (Fig. 12)*

This model differs from the reference model in considering a slower convergence rate that allows the net effect of this parameter for medium crustal strength to be isolated.

The initial development is basically similar to the reference model (Fig. 3) and to the previous model with a mafic granulite lower crust, Vs = 3, Hr = 4 (Fig. 11), except for a major deformation of the plates indicated by a slight bending of the subducting slab at shallow depths, and by a deeply buried lithospheric root and former upper plate margin (44 Ma). At a later stage, however, the indented slab undergoes thermal softening (due to heat diffusion) and, because it is still pushed by the prescribed velocity field it starts to override the left slab (50 Ma). The subduction polarity reversal is furthermore facilitated by a partially melted channel characterized by strong folding of the material that lubricates the main thrust (65 Ma). Notably, a large fraction of rocks composing lower portion of this partially melted channel has a lower crustal origin.

### *3.1.6. Weaker lower crust — Wet Quartzite, Vs = 7, Hr = 5 (Fig. 13)*

Next, for the sake of completion we consider two models with weaker (Wet Quartzite flow law) lower crust with respect to the reference model. The first example is characterized by the same convergence rate as in the reference model.

Extremely weak lower crustal strength manifests itself through the buckling of the upper plate before collision (14 Ma), a marked bending of the indented slab at shallow depths (28 Ma) and the strong delamination

of the lower crust that is scraped off from the subducting slab and accreted in the collisional wedge (40 Ma). The final structure is that of a narrow and thick symmetric two-sided collisional zone delimitated by two down-dipping slabs and characterized by diffuse deformation and partial melting.

*3.1.7. Weaker lower crust and slower convergence rate — Wet Quartzite, Vs = 3, Hr = 4 (Fig. 14)*

The second example of a model with weak lower crust has a slower convergence rate compared to both the reference model and the previous one.

The *complementary effects* of weaker lower crust and slower convergence rate, both of which favor overriding plate bending, result in the extreme case of two-sided orogenic geometry (Fig. 14). After the upper plate yields (22 Ma), the underthrusting slab cannot subduct much further because of the strong rheological coupling between the plates that is mainly due to the low shear heat production along the plate interface at the prescribed slow convergence rate. The indented slab assumes, then, an arcuate shape (28 Ma), until it overcomes the upper plate resistance and one slab rolls over the other (35 Ma). The development of a low viscosity channel made up of sediments, upper and lower crustal units, and partially molten zones between the plates favors rolling. This process, hence, results in a "leaking" of the orogenic root and can accommodate a large amount of convergence with the consumption of a considerable volume of continental crustal material dragged into the deep mantle (44 Ma).

*3.1.8. Stronger lower crust and faster convergence rate — mafic granulite, Vs = 10, Hr = 4 (Fig. 15)*

Finally, we show the results of a model with both a faster convergence rate of 10 cm/a and a stronger lower crust (mafic granulite flow law) compared to the reference model. As can be expected on the basis of the previous analysis, the plates in this model are almost fully rheologically decoupled due to the high viscous heating at the interface.

*Complementary effects* of this decoupling and strong overriding plate resistance to bending lead to the formation of a strongly asymmetric *one-sided* collisional zone (13 Ma) and consumption (subduction) of hundreds of km of continental lithosphere including the entire lower crust.

The general development is similar to the model with the same strong lower crust but slower convergence rate of 7 cm/a (mafic granulite, Vs = 7, Hr = 4) (cf. Fig. 10, 21–42 Ma and Fig. 15, 13–39 Ma) except for the lower extent of up-bending of the overriding plate. However, after 10 Ma (1000 km) of forced convergence followed by 30–35 Ma of spontaneous development associated with downward slab bending and thermal relaxation (compare slab inclination and isotherms in Fig. 15 at 13 and 39 Ma), the subducting slab delaminates from the overriding plate and starts to roll back. This allows for the formation of a hot inter-plate channel (Gerya et al., 2008-this volume) where buoyant crustal and mantle rocks are "regurgitated" rapidly to shallow depths (45 Ma). The buoyant material consists of hot astenospheric mantle and chemically buoyant plumes composed of partially molten subducted lower crustal rocks rising from the top of the slab (Gerya and Yuen, 2003b) subjected to thermal relaxation at 200–300 km depth.

The orogenic wedge is, then, characterized by an extensional regime in the retro-foreland, where molten rocks rise through the hot channel and form domal and diapiric structures (48 Ma), and by a compressional regime on the pro-foreland, where upper crustal material is thrusted toward the foreland (see the black arrows at 47 and 48 Ma).

### *3.2. Summary of the characteristic features of the models*

In all numerical experiments, the initial evolution during subduction of the oceanic slab is very similar where the lithospheric mantle of the overriding plate spreads and thins over the downgoing slab, the upper lithosphere is warped upward and the lower lithosphere is dragged or "ablated" downward (Tao and O'Connell, 1992) — the amount of lithospheric mantle dragging depends on how much the two plates are rheologically coupled.

At the onset of continental collision, the thick sedimentary layer lying on the passive margin of the subducting plate is accreted in the accretionary prism with the uptilted lithospheric edge acting as a buttress. The sedimentary units then transmit the horizontal stresses of the moving plate to the upper lithospheric body that is pushed backward and vertically tilted. Furthermore, with ongoing subduction the lower continental plate resists sinking due to the intrinsic buoyancy of the continental crust, even though it is still constantly pushed from the back by the imposed velocity field and pulled down by the negatively buoyant subducted oceanic slab. The overall effect of these processes then is to increase the horizontal displacement component.

From this stage onward, the model evolution splits into two main orogenic styles, depending on (a) the capacity of the thinned upper plate to counteract the increased

horizontal stress component and (b) the rheological coupling between the two plates defined by the effective strength of rocks composing the plate interface: (1) *asymmetric* (*one-sided*) collision system and (2) *symmetric* (*two-sided*) collisional zone (see Fig. 17 for different orogenic styles). We describe below the evolution of these two main orogenic styles and discuss the most important geodynamic processes (crustal recycling, subduction polarity reversal, rolling over of the plates, etc.) related to the development of post-subduction collisional orogens in our numerical experiments.

### 3.2.1. One-sided collisional zones

If the plates are efficiently decoupled through the rheologically weak interface (caused by shear heating due to high convergence rate) and the overriding lithosphere is strong enough (this crucially depends on the lower crust having high strength) to sustain stresses imposed by the subducting plate, a relatively *broad and thin one-sided* asymmetric collisional zone stabilizes after the onset of collision. Here a vertical upper lithospheric body divides two crustal wedges with different characteristics (Figs. 10 and 15). The prowedge is dominated by simple shear deformation with corner flow-like circulation of the material where the lithospheric body acts as a backstop for the accretionary prism. A midcrustal partially molten level forms and propagates in the direction opposite to that of the converging lower plate triggering exhumation of an inverted metamorphic sequence.

On the other hand, the retrowedge, being mechanically isolated from the shearing of the subducting plate, is characterized by pure shear thickening due to the clockwise rotation of the sub-vertical lithospheric body; here the extent of partial melting is lower because of the absence of highly radiogenic sediments of the passive margin and rocks experience exhumation or burial depending on their position relative to that of the active margin.

### 3.2.2. Two-sided collisional zones

Thinned overriding lithosphere with low-medium crustal strength fails under compressive forces applied by the subducting plate (Figs. 3, 7, and 12–14); however, for low convergence rates, even a lithosphere with a stiff lower crust buckles because of the strong interaction (rheological coupling) of the plates (mafic granulite, Vs=3, Hr=4, Fig. 11). The vertical lithospheric wedge yields and is then dragged downward and embedded between the plates in the lithospheric root; a relatively *narrow and thick two-sided* symmetric collisional zone develops with pro- and retro deformation areas that are delimited by two-sided downdipping plates.

A broad mushroom-shaped, partially molten, midcrustal zone forms because of the thick pile of radiogenic sediments accumulated in the orogenic wedge. Gravitation instabilities inside the partially melted channel trigger the vertical and lateral extrusion of medium-to-high grade metamorphic rocks, with the emplacement of domal and diapiric structures in the central part of the chain, and of an inverted metamorphic sequence on the pro-side of the orogen where HP-MT rocks lie on top of LP-LT units.

### 3.2.3. Crustal recycling

All of the models show that a substantial part of the continental crust is subducted into the mantle and detached from the slab to be recycled (here the term *recycling* refers to the re-incorporation of crustal material into the mantle).

The buckling of the overriding plate produces a two-sided collisional zone that can remain stable throughout the simulation or be followed by slab breakoff, subduction polarity reversal or roll over of the plate. Considerable quantities of the upper as well as lower crust of both plates can be dragged into the deeper mantle or embedded in the lithospheric root during these processes. On the other hand, if the plates are efficiently rheologically decoupled, the lower slab continues to subduct even without external forcing due to slab pull and the scraping off of the buoyant upper part (upper crust). In both of these cases, volumes of consumed crust are to be taken as minimum estimates because these numerical models do not account for phase transformations occurring at transitional depths (>150–200 km).

There are two major implications of these results for global crustal evolution and tectonic reconstruction of orogenic belts. First, the substantial volume of crustal material that is recycled, depending on the details of the collisional process, needs to be considered in models of overall crustal growth and evolution over geological time. These models provide the geodynamic settings in which the varied and widespread isotopic signatures (e.g. Pb, O) of recycled continental material that are found in oceanic basalts have their origin (Weis et al., 2001; Eiler et al., 2000).

The second major implication is in the reconstruction of global tectonic scenarios. It has been noted for some time now that extents of post-collisional convergence (e.g. ca. 2500 Km for the Himalayas, Achache et al., 1984; Patriat and Achache, 1984 etc.) and the degree of shortening estimated from that (ca. one half to

one third, Lyon-Caen and Molnar, 1985; DeCelles et al., 1998) fall far short of observed shortening (e.g. 600–700 Km or less for the Himalaya, DeCelles et al., 2001; Svrivastava and Mitra, 1994; Coward and Butler, 1985; Schelling, 1992) in orogenic belts. In particular, DeCelles et al. (2001) make the key observation that the exposed rocks are largely supracrustal, leaving a large volume of lower crustal material unaccounted for. The widespread delamination and slab break-offs in our models may provide some of the "missing link".

### 3.2.4. Subduction polarity reversal and rolling over of the plates

Several numerical experiments have revealed the development of a symmetrical two-sided collision zone characterized by the indentation of the lower plate on the upper one (e.g., mafic granulite, Vs=3, Hr=4; plagioclase, Vs=3, Hr=5; Wet Quartzite, Vs=7, Hr=5; Wet Quartzite, Vs=3, Hr=4, Figs. 11–14, respectively). Since the yielded upper plate and the underlying lithospheric root offer resistance to any further movement of the subducting plate, collision is halted and isotherms begin to relax. Therefore, at a later stage the material undergoes thermal weakening, especially where stress and, thus, shear heating is larger. If the lower plate is able to overcome the softened resistance along the thrusting plane, subduction is reactivated by the rolling over of both plates that leads to the leakage of a considerable volume of crustal material (Wet Quartzite, Vs=3, Hr=4, Fig. 14).

On the other hand, thermal softening occurring at the indentation zone can favor the yielding and crosscutting of the indented slab followed by a polarity reversal of subduction (plagioclase, Vs=3, Hr=5, Fig. 12), a process also systematically identified in other numerical experiments on the evolution of convergent continental boundaries (e.g. Pysklywek, 2001). Simulations performed with the same strength of the lower crust and convergence velocity but with different rates of internal heat production demonstrate that the timing of subduction polarity reversal is a function of radioactive heat generation, Hr, with lower Hr values resulting in delayed yielding (Fig. 16).

Nevertheless, in both cases the dislocation is "lubricated" by a sandwiched and thermally isolated low viscosity channel made up of sedimentary, upper and lower crustal units which can also be partially molten.

### 3.2.5. Late-collisional hot channel

Rolling back of the subducting slab was observed in mafic granulite, Vs=10, Hr=4 (Fig. 15), where the plates are completely decoupled and the lower one is spontaneously pulled downward by the negative buoyancy of the attached subducted slab. Slab retreating produces a late-collisional hot channel where the buoyant material (astenospheric mantle and partially molten crustal rocks) can escape up to crustal depths. At shallow depths two different tectonic regimes coexist: extension on the backside of the orogenic wedge allows formation of diapiric and domal structures, whilst compression on the pro-side is highlighted by leftward thrusting of upper crustal units.

The formation of hot channels that allow the "regurgitation" of partially molten rocks was already recognized by Gerya et al. (2008-this volume), in an early-collisional tectonic setting. Our results suggest that even at late stages of continental collision transient hot channel effects can appear due to roll back of the subducting plate.

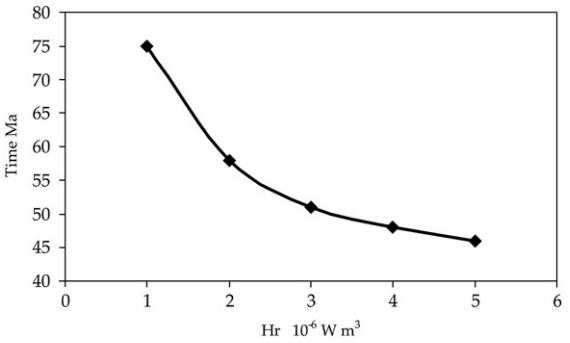


Fig. 16. Timing of subduction polarity reversal vs. internal heat production rate (Hr) in passive margin sediments for lower crustal rheology given by the plagioclase flow law and a convergence velocity of 3 cm/a. Subduction polarity reversal is delayed for low Hr values.

### 3.3. Influence of the studied parameters

We have focused our study on how crustal rheology, convergence velocity and radiogenic heat production rate can influence an evolving post-subduction collisional region with changing styles of orogeny (see Fig. 17):

1. *Lower crustal rheology.* Despite the heterogeneity that is characteristic of the crustal layer of the lithosphere and is very difficult to represent in numerical models, we have shown that a "strong" lower crust (mafic granulite flow law) is able to sustain stresses arising from continental collision so that an asymmetric collisional zone may develop. However, in case of strong coupling at the base of the lithosphere (e.g., due to slow convergence rate and related weak shear heating at the plate interface), vertical forces overcome the plastic yield strength of

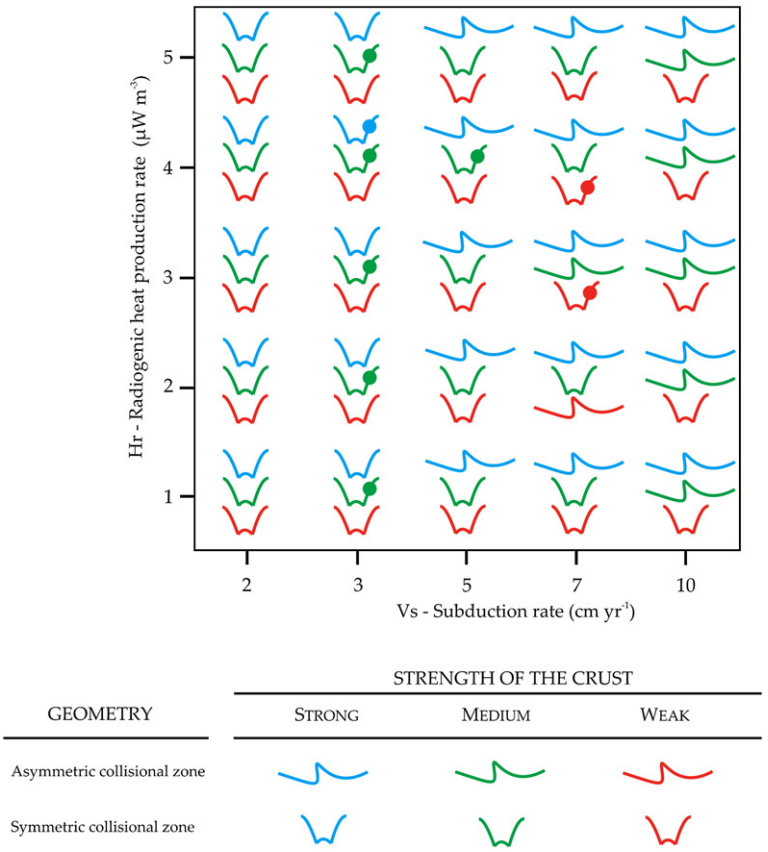


Fig. 17. Different orogenic styles as a function of subduction rate (Vs), radiogenic Heat production rate (Hr), and lower crustal strength. Symbols with a filled dot on the right side indicate models where subduction polarity reversal was observed. Models with an intermediate crustal strength (green color, plagioclase flow law) and Vs=3 were used to calculate timing of subduction reversal polarity as a function of Hr (Fig. 16).

the thinned plate that buckles. "Medium" and "weak" lower crust (plagioclase $An_{75}$ and Wet Quartzite flow laws, respectively) yield in almost all numerical experiments, except in a few simulations with high convergence rates where an asymmetric geometry of the orogen is achieved.

2. *Convergence velocity.* Due to the weakening effect of shear heating the changes in convergence velocity strongly modify rheological coupling at the plate interface. This coupling seems to be the most important parameter that affects styles of post-subduction collisional orogeny, because it determines the magnitude of shearing forces applied to the overriding plate and, consequently, the extent of ablation of lithospheric material. The term "ablation" is used in the sense of the original definition used by Tao and O'Connell, 1992, to describe the downward dragging of lithospheric material due to viscous shearing imposed by the down going plate. In their case the rate of ablation is a function of plate buoyancy, but the results of our numerical experiments show that the rate of ablation also depends strongly on the magnitude of coupling and on the strength of the crust. Frictional heating produced at the shearing interface influences coupling — for low velocities where small stress/strain values are achieved, a huge amount of lithosphere of the overriding plate is tectonically eroded. On the other hand, high velocities produce high shear heating so that the plates are almost completely detached and only a small portion of the upper plate continental lithosphere is dragged downward. However, it should be noted at this point that these models are representative of high friction at the base of the upper plate because dehydratation processes are not included. Including water-releasing reactions followed by overriding plate hydration and resulting rheological weakening (e.g. Gerya and Stöckhert, 2006) in the models could indeed reveal

a different (e.g. reduced upper plate upwarping and erosion) pre-collisional dynamic of the systems.

3. *Radiogenic heating*. The obvious effect of radiogenic heat production rate of sediments is to influence the thermal structure of an orogen. Our models consider only one melting reaction for the bulk crustal material so that at a given limit, increased radiogenic heating enhances only the volume of partially molten rocks without affecting peak temperatures (see P-T-t paths of Figs. 3 and 7). This occurs because all the additional heat is consumed for the phase transition as latent heat. Therefore, volumes of partially molten material observed in our simulations are to be considered upper boundaries of what may be expected in real rock aggregates.

   The stability of the wedge can be related to the gravitational redistribution process (Gerya et al., 2001, 2004b) triggered by partial melting: buoyant and weak partially molten rocks become unstable at depth and move rapidly to the surface, resulting in decompression and cooling. Indeed, P-T-t paths and metamorphic isograd images of models with different Hr content (plagioclase, Vs=7, Hr=5 and plagioclase, Vs=7, Hr=2, Figs. 5, 6 and 8, 9, respectively) indicate that thermal evolution is delayed by several Ma for smaller Hr values. Furthermore, subduction polarity reversal (Fig. 16) and slab detachment (28 Ma for plagioclase, Vs=7, Hr=5 and 40 Ma for plagioclase, Vs=7, Hr=2, Figs. 4 and 7b, respectively) seem to be affected by the concentration of radiogenic elements that controls rates of thermal weakening.

## 4. Discussion: Geological observations/comparison with lithospheric scale structures

Results presented in the last section provide an overview of the major styles of post-subduction collisional orogeny and on how these styles can be modified by different combinations of parameters and resulting forces. Further evolution of the numerical experiments is beyond the scope of this study and more work is necessary to better constrain the early phases of continental collision — for example, by including water release of the downgoing oceanic slab (e.g. Gerya et al., 2008-this volume). Our models are not prescribed for any individual orogen and the images presented here have to be treated as snapshots representing general lithospheric scale development of collisional margins.

What we have learnt from these experiments is that partially molten mid-crustal levels are likely to exist in any region of thickened continental crust provided sufficient radiogenic heating is available. The volume and time of appearance of partial melting is mainly controlled by the radiogenic element content. Once a significant amount of partially molten material is formed, extrusional channel flow and dome structures develop and exhume to the surface as high grade metamorphic rocks. The overall trend is that metamorphic grade increases toward the core of the mountain belt.

Upper plate stresses depend basically on plates coupling and on what material is entering the trench. Rheological coupling turned out to be an important aspect of plate boundaries interaction because determines the amount of stress that is transferred from the lower to the upper plate. Furthermore, as the continental lithosphere is refractory to subduct, even under an imposed velocity field, the horizontal compressive component acting on the upper plate increases when the two continents collide. The combination of these forces together with the lithospheric strength affect the style of collision. When the plates are poorly locked, an asymmetrical one-sided collisional zone forms; on the other hand, if two plates are strongly rheologically coupled, upper slab erosion due to oceanic subduction and subsequent collision give rise to a symmetric two-sided collisional zone with a large lithospheric root. Other authors (e.g. Pfiffner et al., 2000) have shown that two-sided symmetrical crustal orogenic structures can form with a one-sided collisional zone; therefore, to apply our results to symmetric orogens additional constraints on the geometry of the colliding plates are needed on a lithospheric scale.

Having noted this pattern of general behavior, direct comparison of our results to details of specific geological settings is hazardous because:

1. The complexity of natural systems (i.e. material heterogeneity and tectonic inheritance) is difficult to reproduce.
2. The timescale of major plate tectonics processes such as oceanic subduction and subsequent continental collision is of the order of tens or hundreds of Ma, whilst our models address relatively short time scale dynamics. In other words, in real systems later events would be superposed on features that may have been produced at the stage of orogeny simulated in our models.
3. Present-day subduction (Andean-type) and collisional orogens where a reasonable amount of geological and geophysical data are available are the result of long term *complicated and evolving* tectonic activity; therefore, our *relatively simple* post-subduction collision models can reflect only in part the geological evolution of “mature” orogens.

In spite of these potential pitfalls, however, we find that certain gross scale features of real collisional zones (both, Andean- as well as Alpine-type active margins) show intriguing similarities with the results of our numerical experiments.

### 4.1. Andean-type subduction margins

For example, a general aspect of the oceanic subduction phase of our models is that the overriding plate is thinned and spread over the shearing interface so that a part of the upper lithosphere is upwarped and a thin mantle slice wedges between the two crustal portions of the plates. Geophysical data of the uppermost lithosphere acquired along the Cascadia subduction zone (Parson et al., 1998; Romanyuk et al., 2001) and the Central Andes (ANCORP working group, 2003) reveal the presence of a thin lithospheric mantle wedge lying directly in contact with the subducting oceanic crust at shallower depths with respect to neighbouring regions. These observations are made in two active margins that are the result of long term subduction and have different geodynamical settings in terms of velocity of the subducting oceanic slab and upper plate erosion (Central Andes)/accretion (Cascadia). This indicates that mantle wedging occurs regardless of the specifics of dynamic of a subduction zone, consistent with observations from our numerical models. Indeed, the fact that the hangingwall of a reverse fault is thrusted upward should not really be surprising, bearing in mind that the mantle at shallow depths is expected to be rigid with a brittle-plastic behavior.

Our simulations exaggerate the mantle wedging because of the absence in our models of dehydration reactions that would decrease friction between the plates. Detailed sections of other subduction zones as well as models incorporating weakening effects of hydration reactions are required to quantitatively apply the numerical models to specific settings. Nevertheless, lithospheric mantle wedging seems to occur in Andean-type active margins and the degree of the process can be related, to a first order, to the frictional properties along the interface between the plates.

### 4.2. Alpine-type collisional margins

For discussing similarities between collisional, Alpine-type orogens and our model results, we focus our attention to selected aspects of two intensively studied mountain belts — the Himalayan range and the western Alps.

#### 4.2.1. Himalaya

The best example of an active continental collision zone is provided by the Himalayan range where the Indian and the Asian plates are currently colliding. The tectonic evolution that we have calculated using our reference model (plagioclase, Vs = 7, Hr, 5, Figs. 3–6) succeeds in reproducing a number of key observations in the Himalayan range, as follows:

(i) It is necessary to find a suitable heat source to generate temperatures high enough to cause melting, as found ubiquitously in the higher Himalayan crystalline sequence all along the Himalayan range. The inference of Cattin and Avouac (2000) that the presence of radiogenic heat sources are implied from their analysis of the seismic and geomorphologic data has already been noted. Specifically for the Sikkim–Kangchenjunga region, Searle and Szulc (2005) points out that the structural data does not favor melting by decompression, and that an alternate additional heat source, e.g. radiogenic sediments would be more consistent with the observations. We have already noted the widespread occurrence of metasediments with high contents of radiogenic elements in the region. Our models incorporating the effects of high heat generation of radiogenic sediments, coupled with heating due to viscous dissipation, have been found to generate adequately high temperatures.

It is important to note that using the measured concentrations of heat generating elements from the region, it was not only possible to obtain the required temperatures but that these temperatures were attained on reasonable timescales (e.g. ~30 Ma after initiation of collision).

(ii) Inverted metamorphic sequences (higher grade rocks at higher structural, and in the case of the Himalaya, topographic, heights) are common along the entire length of the Himalayan chain. Their origin has been enigmatic for a number of reasons — the issue of the nature of heat source has already been discussed. There are other aspects that have been the topic of intense debate e.g. the nature of the metamorphic field gradient. Among several issues, the most suitable method for geothermometry and geobarometry has been widely discussed from a thermodynamic (e.g. the choice of thermodynamic data) and kinetic (e.g. which compositions were in equilibrium) standpoint. While lateral variations along strike are entirely possible, at least for profiles in the Sikkim region, thermodynamically and kinetically well constrained thermobarometry indicate (e.g. Dasgupta et al., 2004) that the sequence is one of continuous increase in pressure as well as temperature. The right side down metamorphism (T increasing with P or depth) indicates that the metamorphic

rocks were produced under normal (in direction rather than magnitude) thermal gradients and then inverted. However, the continuity and coherence place stringent constraints on the nature of processes that can be responsible for the inversion and subsequent exhumation — simple combinations of thrusting are unlikely to preserve the coherence and continuity of these metamorphic blocks. The melting triggered inversion and exhumation along mid crustal channels observed in our models provide a suitable mechanism.

(iii) P-T paths and cooling/exhumation rates: Our models further indicate that there is a difference in the shape of the P-T paths for lower (~lesser Himalayas) and higher (~Greater Himalayas) grade rocks, respectively. The rocks corresponding to lesser Himalayan metamorphic grades in our models form a coherent package that undergo a clockwise P-T path. The corresponding "higher Himalayan rocks" form a more mixed package (coming from different depths) of rocks that follow an overall clockwise path as well, but with an initial phase of rapid decompression to mid crustal depths followed by slow cooling and exhumation. This is consistent with observations from the High Himalaya Crystallines in Sikkim as well, where Ganguly et al. (2000) found an initial exhumation rate of 15 mm/yr. that changed to ~2 mm/yr at depths of about 15 km. Variations in P-T paths between lesser and higher Himalayan rocks have also been more widely documented by Goscombe et al. (2006), although they have observed even anticlockwise P-T paths in some of their higher Himalayan samples from Nepal.

Once again, even excluding variations to be expected due to possible along strike variations (Nepal vs. Sikkim) and the maturity of the orogen, details of individual orogens cannot be expected to be reproduced in general models such as the ones of this study. However, the number of salient but enigmatic observed features of the Himalayan collision zone that our models do succeed in reproducing is highly encouraging and provides useful insights.

#### 4.2.2. Western Alps

The western part of the European Alps are characterized by southward subduction of the European plate and indentation of the upper Adria plate, whose northern margin is vertically tilted and outcrops at the surface forming the well-known Ivrea–Sesia Zone (ISZ).

In the Late Carboniferous to Early Permian a major pulse of basic magmatic underplating (called "Mafic Complex") occurred in the lower crustal section of the ISZ during an extensional regime initiated after the Variscan collision (Handy and Zingg, 1991). Radiometric data (Vavra et al., 1999 and references therein) show that the Ivrea Zone cooled below 300 °C at around 180 Ma indicating that the Moho was probably at 20–25 km of depth. This means that the margin was already slightly upbended before the final exhumation occurred during the Alpine orogeny.

Today, the Western Alps are an asymmetric collisional zone with two crustal wedges separated by the vertical lithospheric body; the northern wedge (or pro-wedge) is dominated by nappe stacking, faulting and folding, whilst the southern wedge (or retrowedge) by crustal thickening and backthrusting of the crust (Schmid and Kissling, 2000). The Alps includes ophiolites that are embedded in high grade metamorphic nappes (Schmid et al., 2004) and are bounded southward by the northern margin of Adria or ISZ that acted as a backstop and allowed the exhumation of the deeper levels of the orogenic wedge. Gerya and Stöckhert, 2006, have argued that such a complex mixing of different lithotypes could in part be related to pre-collisional subduction processes (which is also in line with our experiments demonstrating strong mixing of rocks in the accretion wedge during subduction, Fig. 10, 10–15 Ma) and predicted that continental collision together with erosion could bring high-pressure metamorphic rocks to the surface.

Simulations with a rigid lower crust (i.e. mafic granulite, Vs=7, Hr=4, Fig. 10) seem, indeed, to match many large scale geological aspects of the Western Alps: the asymmetry of the orogen is characterized by the vertical lithospheric margin of the (Adria) overriding plate that separates two distinct crustal wedges with different metamorphic and deformation patterns. In the pro-wedge, high grade metamorphic rocks of continental upper crust and oceanic (blue square of Fig. 10) material are mixed together and exhumed up to the surface by a corner-flow like mass circulation accentuated by gravitational instabilities due to partial melting. The mafic continental crust is almost completely consumed at the active margin, so that the upper and lower parts of the crust seem to be decoupled (Bousquet et al., 1997).

The model of Fig. 10 includes passive margin sediments with high radiogenic heating (Hr=4 W/m$^3$) that probably produce a higher quantity of partial melting than what is observed in the Western Alps. Simulations with a lower content of radiogenic elements of the passive margin sediments show a cooler thermal structure of the orogen (e.g. Goffe et al., 2003) that could be more applicable to this region. The rheology used (mafic granulite flow law) in the model could account for the Permian basic intrusion ("Mafic Complex") surviving at this high level. The rheology

causes the upbended rigid plate margin to achieve such a vertical position instead of being buckled down and buried in the lithospheric root. Crustal thickening and backthrusting is more dominant in the southern wedge, as would be expected from our models.

## 5. Conclusions

In the present study we systematically modeled in 2-D the evolution of post-subduction collisional orogens which are representative for the cases where negligible slab dehydration occurs during the final stages of subduction. The most important aspects of this study can be summarized in the following points:

1. Oceanic subduction produces upper plate erosion and upbending (mantle wedging), the extent of which depends on the rheological coupling between plates.
2. Slow convergence rates (weak shear heating and consequently strong rheological coupling between plates) and/or a weak lithosphere produces plastic yielding of the upper slab and results in the formation of a two-sided post-subduction collision zone characterized by a symmetric orogenic style on both crustal and plate scale, a narrow and thick collisional zone and lateral-vertical extrusion of an inverted metamorphic sequence.
3. High convergence rates (strong shear heating and consequently weak rheological coupling between plates) and a strong lithosphere produce a broad and thin asymmetrical one-sided post-subduction collisional zone with two distinct wedges separated by a sub-vertical lithospheric body and characterized by different deformation regimes; in the pro-wedge, simple shear deformation is indicated by corner flow-like mass circulation with lateral extrusion of an inverted metamorphic sequence. The retrowedge, on the contrary, thickens by means of pure shear mechanism with almost vertical exhumation/burial of rocks and likely presence of shallow depth backthrusts that accommodate the clockwise rotation of the lithospheric body.
4. Peak temperature record of medium-to-high grade metamoprhic rocks indicates lateral extrusion (toward the pro-foreland) of a coherent HP-MT body on a LP-LT unit, whilst peak pressure signature of the higher grade rocks reveals mixing from different depths (15–23 kbar, >700 °C).
5. Crustal recycling into the deep mantle is a very common aspect of post-subduction continental collision. This implies that models of crustal growth and evolution need to take this flux into account. Moreover, this lost mass may account for much of the mismatch between inferred extents of convergence and shortening.
6. Late evolution of several models have shown the formation of lithospheric structures like polarity reversal or rolling over of the plates, as already recognized by other authors (i.e., Pysklywek, 2001). The appereance of a late-collisional transient hot channel due to the roll back of the subducting plate extends the results presented in Gerya et al. (2008-this volume), where the formation of hot channels is found in early-collisional settings, and gives important insights on coupled extensive/compressive tectonic regimes.
7. Radiogenic heating controls the thermal structure and evolution of collisional zones with the volume of partially molten rocks, the timing of exhumation of the inverted metamorphic sequence and the onset of slab yielding phases (like subduction polarity reversal or slab breakoff) being a function of radiogenic element concentration of the passive margin sediments.
8. We found interesting similarities between model results and features of real orogens such as the pre-collisional subduction-related systems (Cascadia and Central Andes subduction zones) and post-subduction collision-related chains (Himalaya and Western Alps). The model results provide a mechanism for producing the inverted metamorphism observed in the Himalaya, matching aspects of detail such as coherence of the sequence, shapes of P-T paths at different grades and timing and duration of metamorphism observed in certain parts. More detailed lithospheric images of collisional orogens are needed to derive better constrained models for specific orogens. However, we believe our results provide important links between lithological assemblages and geodynamics that can help to infer processes that led to observed petrological features.

## Acknowledgements

This work was supported by ETH Research Grants TH-12/04-1, TH-12/05-3, SNF Research Grant 200021-113672/1 and by the RF President Program “Leading Scientific School of Russia” (grant # НШ-5338.2006.5 to TVG) and the RFBR grant # 06-05-64098 (to TVG). The research of SC was generously supported by the German Science Foundation (DFG) under various programs, including the SFB 526 (Rheology of the Earth). We thank Romain Bousquet and Nina Kukowsky for their helpful and constructive reviews.

## Appendix A

*Initial model geometry and setup*

We used the 2D finite difference code I2VIS with a marker-in-cell technique which allows for nondiffusive numerical simulation of multiphase flow in a rectangular fully staggered Eulerian grid (Gerya and Yuen, 2003a). The grid is nonuniform, with a resolution varying from 2×2 km in the studied collisional zone to 30×30 km away from it. The 4000×670 km box (Fig. 2) contains around 7 million markers and has free slip boundaries and a permeable lower boundary with an infinity-like external free slip and external constant temperature conditions at 1670 km of depth (Burg and Gerya, 2005; Gerya et al., 2008-this volume). A spontaneously bending plate is pushed rightward by an internal prescribed velocity field that remains fixed with respect to the Eulerian coordinates. After around 1000 km of convergence the strong lithospheric part of the subducting plate leaves the prescribed velocity domain and plate movement becomes spontaneous, being regulated by subducted slab pull and by rheological coupling along the plate interface.

The initial setup of the models implies an early stage (5 Ma after nucleation) oceanic/continental subduction with a 50 to 5 km thick and down to 155 km (below the bottom of the crust) zone of weakness (serpentinized subduction channel, Gerya and Stöckhert, 2006) that has a wet olivine rheology and low plastic strength. The initial steady state thermal structure of the lithosphere corresponds to specific radiogenic heat production in the crust, $T$=0 °C at the surface and $T$=1350 °C condition at 150 km depth. An 800 km wide oceanic slab is attached to a continental passive margin plate with a 400×10 km layer of highly radiogenic sediments. Continental crust is divided into a 20 km upper and a 15 km lower crustal layer, whilst oceanic crust is 8 km thick. The material properties of all layers are shown in Table 1.

*Topography*

The spontaneous deformation of the upper surface, i.e. topography, is calculated dynamically as a free surface by using a low viscosity ($10^{19}$ Pa s) 10–14 km thick layer made of "air" (1 kg/m$^3$, above $z$=10 km sea level) or "water" (1000 kg/m$^3$, below $z$=10 km sea level). The interface between this weak layer and the underlying crust is treated as an erosional/sedimentation surface which evolves according to the transportation equation solved in Eulerian coordinates at each time step (Gerya and Yuen, 2003b):

$$\partial z_{es}/\partial t = v_z - v_x \partial z_{es}/\partial x - v_s + v_e \quad (1)$$

Here $z_{es}$ is the vertical position of the surface as a function of the horizontal distance $v_x$; $v_z$ and $v_x$ are the vertical and horizontal components of the material velocity vector at the surface; $v_s$ and $v_e$ are the sedimentation and erosion rates, respectively, which correspond to the relation:

$$\begin{aligned} v_s &= 0\,\text{mm}/a, \quad v_e = v_{e0} \quad \text{when } z_{es}<10\,\text{km} \\ v_s &= v_{s0}\,\text{mm}/a, \quad v_e = 0 \quad \text{when } z_{es}>10\,\text{km} \end{aligned}$$

where $v_{e0}$ and $v_{s0}$ are the imposed constant erosion and sedimentation rates, respectively. The code allows for marker transmutation that simulates erosion (rock markers are transformed to weak layer markers) and sedimentation (weak layer markers are transformed to sediments).

*Rheological model*

A viscoplastic rheology is assigned to the model by means of a Christmas tree-like criterion, where the rheological behavior depends on the minimun differential stress attained between the ductile and brittle fields (Ranalli, 1995).

Viscous rheology for rocks containing small melt fractions ($M$<0.1) is determined by flow laws (Table 1), where the effective creep viscosities are a function of strain rate, pressure and temperature. The effective viscosity of molten rocks ($M$>0.1) was calculated using the formula (Pinkerton and Stevenson, 1992; Bittner and Schmeling, 1995):

$$\eta = \eta_0 \quad \exp\left[2.5 + (1-M)\left(\frac{1-M}{M}\right)^{0.48}\right] \quad (2)$$

Here $\eta_0$ is an empirical parameter depending on rock composition, being $\eta_0=10^{13}$ Pa s for molten mafic rocks and $\eta_0=5\times10^{14}$ Pa s for molten felsic rocks.

The strength of solid rocks in the brittle field is implemented as a limiting maximum viscosity

$$\eta_{max} = \left(\frac{\frac{1}{2}\sigma_{yield}}{(\varepsilon_{II})^{1/2}}\right) \quad (3)$$

where $\varepsilon_{II}$ is the second invariant of the strain rate tensor, $\sigma_{yield}=(N_1 P_{lith}+N_2)(1-\lambda)$ is the yield stress, $P_{lith}$ is the lithostatic depth dependent pressure; N1 and N2 are

empirical constants (Brace and Kohlstedt, 1980); $\lambda$ is the pore fluid coefficient that varies with depth beneath the calculated topographic surface ($\Delta z_{\mathrm{Topo}}$) according to the formula (Gerya and Stöckhert, 2006):

$$\lambda = \frac{\lambda_0(10 - \Delta z_{\mathrm{Topo}}) + \lambda_{10}\Delta z_{\mathrm{Topo}}}{10} \quad \text{when } 0 \le \Delta z_{\mathrm{Topo}} \le 10\ \mathrm{km}$$

$$\lambda = \lambda_{10} \quad \text{when } \Delta z_{\mathrm{Topo}} > 10\ \mathrm{km}$$

where $\lambda_0$ is the hydrostatic pore pressure (0.4) at the surface, and $\lambda_{10}$ is the pore fluid pressure at 10 km depth ($\lambda_{10}$=0.9 for sediments and hydrated mantle and $\lambda_{10}$=0.5 for all other rocks). The model allows for strain localization due to the thermal weakening effects of shear heating (i.e. without prescribing strain softening of the lithologies).

*Partial melting*

The numerical code accounts for partial melting of the various lithologies by using experimentally obtained P-T dependent wet solidus and dry liquidus curves (Table 1). Volumetric melt fraction $M$ is assumed to increase linearly with temperature accordingly to the following relations (Burg and Gerya, 2005):

$$M = 0 \text{ at } T \le T_{\mathrm{solidus}}, \tag{4}$$

$$M = \frac{(T - T_{\mathrm{solidus}})}{(T_{\mathrm{liquidus}} - T_{\mathrm{solidus}})} \text{ at } T_{\mathrm{solidus}} < T < T_{\mathrm{liquidus}} \tag{5}$$

$$M = 1 \text{ at } T \ge T_{\mathrm{liquidus}} \tag{6}$$

where $T_{\mathrm{solidus}}$ and $T_{\mathrm{liquidus}}$ are the wet solidus and dry liquidus temperature of the given lithology.

Consequently, the effective density, $\rho_{\mathrm{eff}}$, of partially molten rocks varies with the amount of melt fraction and P-T conditions according to the relations:

$$\rho_{\mathrm{eff}} = \rho_{\mathrm{solid}} - M(\rho_{\mathrm{solid}} - \rho_{\mathrm{molten}}) \tag{7}$$

$$\rho_{P,T} = \rho_0[1 - \alpha(T - T_0)][1 + \beta(P - P_0)] \tag{8}$$

where $\rho_{\mathrm{solid}}$ and $\rho_{\mathrm{solid}}$ are the densities of the solid and molten rock, respectively, $\rho_0$ is the density at $P_0$=0.1 MPa and $T_0$=298 K; $\alpha$ and $\beta$ are the thermal expansion and compressibility coefficients, respectively.

The effects of latent heat are accounted for by an increased effective heat capacity ($\mathrm{Cp_{eff}}$) and thermal expansion ($\alpha_{\mathrm{eff}}$) of the partially molten rocks ($0<M<1$), calculated as

$$\mathrm{Cp_{eff}} = \mathrm{Cp} + Q_{\mathrm{L}}\left[(\partial M/\partial T)_{\mathrm{P}}\right], \tag{9a}$$

$$\alpha_{\mathrm{eff}} = \alpha + \rho Q_{\mathrm{L}}\left[(\partial M/\partial P)_{\mathrm{T}}\right]/T, \tag{9b}$$

where Cp and $\alpha$ are the heat capacity and the thermal expansion of the solid crust, respectively, and $Q_{\mathrm{L}}$ is the latent heat of melting of the crust.

*Numerical approach*

The thermal, momentum and continuity equations. for a 2D creeping flow, including thermal and chemical buoyant forces, are solved using the I2VIS code (Gerya and Yuen, 2003a). The thermal equation has the form of:

$$\begin{aligned} &\rho C_{\mathrm{p}}\left(\frac{DT}{Dt}\right) = -\frac{\partial q_x}{\partial x} - \frac{\partial q_z}{\partial z} + H_{\mathrm{r}} + H_{\mathrm{a}} + H_{\mathrm{S}} + H_{\mathrm{L}} \\ &q_x = -k(T,P,C)\frac{\partial T}{\partial x} \qquad q_z = -k(T,P,C)\frac{\partial T}{\partial z} \\ &H_{\mathrm{a}} = T\alpha\frac{DP}{Dt} \qquad\qquad H_{\mathrm{S}} = \sigma_{xx}\varepsilon_{xx} + \sigma_{zz}\varepsilon_{zz} + 2\sigma_{xz}\varepsilon_{xz} \end{aligned} \tag{10}$$

where $D/Dt$ is the substantive time derivative; $x$ and $z$ denote, respectively, the horizontal and vertical directions; the deviatoric stress tensor is defined by $\sigma_{xx}$, $\sigma_{xz}$, $\sigma_{zz}$, whilst the strain rate tensor is defined by $\varepsilon_{\mathrm{xx}}$, $\varepsilon_{\mathrm{xz}}$, $\varepsilon_{zz}$; $T$ is the temperature, $P$ the pressure and $C$ the composition; $q_x$ and $q_z$ are heat flux components; $\rho$ is the density, $k(T,P,C)$ is the thermal conductivity as a function of temperature, pressure and composition (e.g. Hofmeister, 1999), $C_{\mathrm{p}}$ is the isobaric heat capacity; $H_{\mathrm{r}}$, $H_{\mathrm{a}}$, $H_{\mathrm{S}}$, $H_{\mathrm{L}}$ are, respectively, radioactive, adiabatic, shear and latent heat production ($H_{\mathrm{L}}$ is implemented by changing $C_{\mathrm{p}}$ and $\alpha$ according to Eqs. (9a), (9b)).

Conservation of mass is approximated by the incompressible mass conservation (continuity) equation:

$$\frac{\partial v_x}{\partial x} + \frac{\partial v_z}{\partial z} = 0 \tag{11}$$

The 2D Stockes equation has the form:

$$\frac{\partial \sigma_{xx}}{\partial x} + \frac{\partial \sigma_{xz}}{\partial z} = \frac{\partial P}{\partial x} \tag{12}$$

$$\frac{\partial \sigma_{zz}}{\partial z} + \frac{\partial \sigma_{xz}}{\partial x} = \frac{\partial P}{\partial z} - g\rho(T,P,C,M) \tag{13}$$

where the density $\rho$ depends on temperature, pressure, composition and melt fraction; $g$ is the acceleration due to gravity.

## References


Achache, J., Courtillot, V., Xiu, Y., 1984. Paleogeographic and tectonic evolution of southern Tibet since middle Cretaceous time: new paleomagnetic data and synthesis. J. Geophys. Res. 89, 10311–10339.

ANCORP working group, 2003. Seismic imaging of a convergent continental margin — the central Andes (ANCORP'96). J. Geophys. Res. 108 (B7), 2328.

Beaumont, C., Jamieson, R.A., Nguyen, M.H., Lee, B., 2001. Himalayan tectonics explained by extrusion of a low-viscosity crustal channel coupled to focused surface denudation. Nature 414, 738–742.

Bittner, D., Schmeling, H., 1995. Numerical modeling of melting processes and induced diapirism in the lower crust. Geophys. J. Int. 123, 59–70.

Bousquet, R., Gogge, B., Henry, P., Le Pichon, X., Chopin, C., 1997. Kinematic, thermal and petrological model of the Central Alps: lepontine metamorphism in the upper crust and eclogitisation of the lower crust. Tectonophysics 273 (1), 105–127.

Brace, W.F., Kohlstedt, D.T., 1980. Limits on lithospheric stress imposed by laboratory experiments. J. Geophys. Res. 85, 6248–6252.

Burg, J.P., Gerya, T.V., 2005. The role of viscous heating in Barrovian metamorphism of collisional orogens: thermomechanical models and application to the Lepontine Dome in the Central Alps. J. Metamorp. Geol. 23, 75–95.

Burov, E., Jolivet, L., Le Pourhiet, L., Poliakov, A., 2001. A thermo-mechanical model of exhumation of high pressure (HP) and ultra-high pressure (UHP) metamorphic rocks in Alpine-type collision belts. Tectonophysics 342, 113–136.

Cattin, R., Avouac, J.P., 2000. Modeling mountain building and the seismic cycle in the Himalaya of Nepal. J. Geophys. Res. 105, 13389–13407.

Chamberlain, C.P., Sonder, L.J., 1990. Heat-producing elements and the thermal and baric patterns of metamorphic belts. Science 250, 763–769.

Clauser, C., Huenges, E., 1995. Thermal conductivity of rocks and minerals. In: Ahrens T.J. (Ed.), Rock Physics and Phase Relations, vol. 3. American Geophysical Reunion Shelf, Washington DC, 105–126.

Coward, M.P., Butler, R.W.H., 1985. Thrust tectonics and the deep structure of the Pakistan Himalaya. Geology 13, 417–420.

Dasgupta, S., Ganguly, J., Neogi, S., 2004. Inverted metamorphic sequence in the Sikkim Himalayas: crystallization history, P-T gradient and implications. J. Metamorph. Geol. 22, 395–412.

DeCelles, P.G., Gehrels, G.E., Quade, J., Ojha, T.P., 1998. Eocene-early Miocene foreland basin development and the history of Himalayan thrusting, western and central Nepal. Tectonics 17, 741–765.

DeCelles, P.G., Robinson, D.M., Quade, J., Ojha, T.P., Garzione, C.N., Copeland, P., Upreti, B.N., 2001. Stratigraphy, structure, and tectonic evolution of the Himalayan fold thrust belt in western Nepal. Tectonics 20 (4), 487–509.

Eiler, J.M., Schiano, P., Kitchen, N., Stolper, E.M., 2000. Oxygen-isotope evidence for recycled crust in the sources of mid-ocean-ridge basalts. Nature 403, 530–534.

England, P., Le Fort, P., Molnar, P., Pecher, A., 1992. Heat sources for tertiary metamorphism and anatexis in the Annapurna–Manaslu region Central Nepal. J. Geophys. Res. 97 (B2), 2107–2128.

Ganguly, J., Dasgupta, S., Cheng, W., Neogi, S., 2000. Exhumation history of a section of the Sikkim Himalayas, India: record in the metamorphic mineral equilibria and compositional zoning of garnet. Earth Planet Sci. Lett. 183, 471–486.

Gerya, T.V., Yuen, D.A., 2003a. Characteristic-based marker-in-cell method with conservative finite-differences schemes for modeling geological flows with strongly variable transport properties. Physics of the Earth and Planetary Interiors 140, 295–320.

Gerya, T.V., Yuen, D.A., 2003b. Rayleigh–Taylor instabilities from hydratation and melting propel "cold plumes" at subduction zones. Earth Planet. Sci Lett. 212, 47–62.

Gerya, T.V., Stöckhert, B., 2006. Two dimensional numerical modeling of tectonic and metamorphic histories at active continental margins. Int. J. Earth Sci. (Geol Rundsch) 95 (2), 250–274.

Gerya, T.V., Maresch, W.V., Willner, A.P., Van Reenen, D.D., Smit, C.A., 2001. Inherent gravitational instability of thickened continental crust with regionally developed low- to medium-pressure granulite facies metamorphism. Earth Planet. Sci. Lett. 190, 221–235.

Gerya, T.V., Yuen, D.A., Maresch, W.V., 2004a. Thermomechanical modeling of slab detachment. Earth Planet. Sci. Lett. 226, 101–116.

Gerya, T.V., Perchuk, L.L., Maresch, W.V., Willner, A.P., 2004b. Inherent gravitational instability of hot continental crust: implication for doming and diapirism in granulite facies terrains. In: Whitney, D., Teyssier, C., Siddoway, C.S. (Eds.), Gneiss Domes in Orogeny. GSA Special Paper, 380, pp. 97–115.

Gerya, T.V., Perchuk, L.L., Burg, J.P., 2008. Transient hot channels: perpetrating and regurgitating ultrahigh-pressure, high temperature crust-mantle associations in collision belts. Lithos 103, 236–256 (this volume). doi:10.1016/j.lithos.2007.09.017.

Goffé, B., Bousquet, R., Henry, P., LePichon, X., 2003. Effect of chemical composition of the crust on the metamorphic evolution of orogenic wedges. J. Metamorph. Geol. 21, 123–141.

Goscombe, B., Gray, D., Hand, M., 2006. Crustal architecture of the Himalayan metamorphic front in eastern Nepal. Gond. Res. 10, 232–255.

Handy, M.R., Zingg, A., 1991. The tectonic and rheological evolution of an attenuated cross section of the continental crust — Ivrea crustal section, Southern Alps, Northwestern Italy and Southern Switzerland. Geol. Soc. Amer. Bull. 103, 236–253.

Hofmeister, A.M., 1999. Mantle values of thermal conductivity and the geotherm from phonon lifetimes. Science 283, 1699–1706.

Huerta, A.D., Royden, L.H., Hodges, K.V., 1998. The thermal structure of collisional orogens as a response to accretion, erosion, and radiogenic heating. J. Geophys. Res. 103, 15287–15302.

Huerta, A.D., Royden, L.H., Hodges, K.V., 1999. The effects of accretion, erosion and radiogenic heat on the metamorphic evolution of collisional orogens. J. Metamorph. Geol. 17, 349–366.

Jamieson, R.A., Beaumont, C., Fullsack, P., Lee, B., 1998. Barrovian regional metamorphism: where's the heat? In: Treloar, P.J., O'Brien, P.J. (Eds.), What Drives Metamorphism and Metamorphic Reactions? Geological Society, 138. Special Publications, London, pp. 1–5.

Lyon-Caen, H., Molnar, P., 1985. Gravity anomalies, flexure of the Indian plate, and the structure, support and evolution of the Himalaya and Ganga basin. Tectonics 4, 513–538.

Macfarlane, A.M., 1992. The tectonic evolution of the core of the Himalaya, Langtang National Park, central Nepal, Ph. D. thesis, Mass. Inst. of Technol., Cambridge.

Molnar, P., England, P., 1990. Temperatures, heat flux, and frictional stress near major thrust faults. J. Geophys. Res. 95, 4833–4856.

Neumann, N., Sandiford, M., Foden, J., 2000. Regional geochemistry and continental heat flow: implications for the origin of the south

Australian heat flow anomaly. Earth Planet. Sci. Lett. 183, 107–120.
Nozkhin, A.D., Turkina, O.M., 1993. Geochemistry of granulites. Novosibirsk: Institute of Geology and Geophysics Russian Academy of Sciences Press. (in Russian).
Parson, T., Trehu, A., Luetgert, J.H., Miller, K., Kilbride, F., Wells, R.E., Fisher, M.A., Flueh, E., ten Brink, U.S., Christensen, N.I., 1998. A new view into Cascadia subduction zone and volcanic arc: implications for earthquake hazards along the Washington margin. Geology 26, 199–202.
Patriat, P., Achache, J., 1984. India–Eurasia collision chronology has implications for crustal shortening driving mechanism of plates. Nature 311, 615–621.
Pattino-Douce, A.E., Humphreys, E.D., Johnston, A.D., 1990. Anatexis and metamorphism in tectonically thickened continental crust exemplified by the Sevier hinterland, western North America. Earth Planet. Sci. Lett. 97, 290–315.
Pfiffner, O.A., Ellis, S., Beaumont, C., 2000. Collision tectonics in the Swiss Alps: insight from geodynamic modeling. Tectonics 19 (6), 1065–1094.
Pinkerton, H., Stevenson, R.J., 1992. Methods of determining the rheological properties of magmas at subliquidus temperatures. J. Volcanol. Geotherm. Res. 53, 47–66.
Pysklywek, R.N., 2001. Evolution of subduction mantle lithosphere at a continental plate boundary. Geophys. Res. Lett. 23 (22), 4399–4402.
Pysklywek, R.N., Beaumont, C., 2004. Intraplate tectonics: feedback between radioactive thermal weakening and crustal deformation driven by mantle lithosphere instabilities. Earth Planet. Sci. Lett. 221, 275–292.
Ranalli, G., 1995. Rheology of the Earth. Chapman and Hall, London UK, p. 413.
Romanyuk, T.V., Mooney, W.D., Blakely, R.J., 2001. Cascade subduction zone, North America; a tectono-geophysical model. Geotectonics 35, 224–244.
Rudnick, R., Fountain, D., 1995. Nature and composition of the continental crust: a lower crustal perspective. Rev. Geophys. 33, 267–309.
Scaillet, B.C., France-Lanord, P., Le Fort, P., 1990. Batrinath–Gangotri plutons (Garhwal, India): petrological and geochemical evidence for fractional processes in a high Himalaya leucogranite. J. Volcanol. Geotherm. Res. 44, 163–188.
Schelling, D., 1992. The tectonostratigraphy and structure of the eastern Nepal Himalaya. Tectonics 11, 925–943.
Schmid, S.M., Kissling, E., 2000. The arc of the western Alps in the light of geophysical data on deep crustal structure. Tectonics 19 (1), 62–85.
Schmid, S.M., Fügenshuh, B., Kissling, E., Schuster, R., 2004. Tectonic map and overall architecture of the Alpine orogen. Ecol. Geol. Helv. 07, 93–117.
Schmidt, M.W., Poli, S., 1998. Experimentally based water budgets for dehydrating slabs and consequences for arc magma generation. Earth Planet. Sci. Lett. 163, 361–379.
Searle, M.P., Szulc, A.G., 2005. Channel flow and ductile extrusion of the High Himalayan slab — the Kangchenjunga–Darjeeling profile, Sikkim Himalaya. J. Asian Earth Sci. 25, 173–185.
Svrivastava, P., Mitra, G., 1994. Thrust geometries and deep structure of the outer and lesser Himalaya, Kumaon and Garhwal (India): implications for evolution of the Himalayan fold-and-thrust belt. Tectonics 13, 89–109.
Tao, W.C., O'Connell, R.J., 1992. Ablative subduction: a two-sided alternative to the conventional subduction model. J. Geophys. Res. 97, 8877–8904.
Taylor, S.R., McLennan, S.M., 1995. The geochemical evolution of the continental crust. Rev. Geophys. 33, 241–265.
Turcotte, D.L., Schubert, G., 1982. Geodynamics: Applications of Continuum Physics to Geological Problems. Wiley, New York, p. 450.
Vavra, G., Schmid, R., Gebauer, D., 1999. Internal morphology, habit and U–Th–Pb microanalysis of amphibolite-to-granulite facies zircons: geochronology of the Ivrea Zone (Southern Alps). Contrib. Mineral. Petrol. 134, 380–404.
Vidal, P., Cocherie, A., Le Fort, P., 1982. Geochemical investigations of the origin of the Manaslu leucogranite (Himalaya, Nepal). Geochim. Cosmochim. Acta 46, 2279–2292.
Weis, D., Ingle, S., Damasceno, D., Frey, F.A., Nicolaysen, K., Barling, J., 2001. Origin of Continental Components in Indian Ocean Basalts: Evidence from Elan Bank. Kerguelen Plateau, ODP Leg 183, Site 1137.